



**PREPARATION OF MnO_2 AND $MXene$ DOPED
CARBON CLOTH BASED FLEXIBLE
SUPERCAPACITOR ELECTRODES**

**2023
MASTER THESIS
METALLURGY AND MATERIALS ENGINEERING**

MARIEM ABDI

**Thesis Advisor
Assist. Prof. Dr. Safa POLAT**

**PREPARATION OF MnO_2 AND MXene DOPED CARBON CLOTH BASED
FLEXIBLE SUPERCAPACITOR ELECTRODES**

T.C.

Karabuk University

Institute of Graduate Programs

Department of Metallurgy and Materials Engineering

Prepared as

Master Thesis

Mariem ABDI

Thesis Advisor

Assist. Prof. Dr. Safa POLAT

KARABUK

January 2023

I certify that in my opinion the thesis submitted by Mariem ABDI titled “PREPARATION OF MNO_2 AND MXene DOPED CARBON CLOTH BASED FLEXIBLE SUPERCAPACITOR ELECTRODES” is fully adequate in scope and in quality as a thesis for the degree of Master of Science.

Assist. Prof. Dr. Safa POLAT
Thesis Advisor, Department of Metallurgy and Materials Engineering

This thesis is accepted by the examining committee with a unanimous vote in the Department of Metallurgy and Materials Engineering as a Master of Science thesis.
January 31, 2023

<u>Examining Committee Members (Institutions)</u>	<u>Signature</u>
Chairman : Assoc Prof. Dr. Muhammet Emre TURAN (KBU)
Member : Assist. Prof. Dr. Safa POLAT (KBU)
Member : Assoc. Prof. Dr. Adem YAR (BU)

The degree of Master of Science by the thesis submitted is approved by the Administrative Board of the Institute of Graduate Programs, Karabuk University.

Prof. Dr. Müslüm KUZU
Director of the Institute of Graduate Programs

“I declare that all the information within this thesis has been gathered and presented in accordance with academic regulations and ethical principles and I have according to the requirements of these regulations and principles cited all those which do not originate in this work as well.”

Mariem ABDI

ABSTRACT

M. Sc. Thesis

PREPARATION OF MnO_2 AND MXene DOPED CARBON CLOTH BASED FLEXIBLE SUPERCAPACITOR ELECTRODES

Karabuk University

Institute of Graduate Programs

Department of Metallurgy and Materials Engineering

Mariem ABDI

Thesis Advisor:

Assoc. Prof. Dr. Safa POLAT

January 2023, 60 pages

With the increase in the global population and the increase in research on the development of renewable energy sources, there has been a significant increase in the demand for energy storage systems (EDS). It is known that flexible EDSs are needed in order to meet the needs of consumer electronics such as flexible robots, biosensors and new generation mobile phones with flexible screens, which have been developed in recent years. Supercapacitors are one of the most common EDS used and under development in this regard. In this study, it is aimed to produce carbon fabric-based $MnO_2@MXene$ doped composite electrodes for flexible supercapacitors. For this purpose, current collector conductive and flexible carbon fabrics were used. These are obtained by exposing the cotton fabric to high temperature in an oxygen-free environment. Then, MnO_2 was synthesized by hydrothermal method to functionalize the surfaces of these fabrics. In addition, MXene contributions were made to these syntheses at different rates. The MXene structure was obtained by removing the

aluminum from the MAX ($\text{Ti}_3\text{Al}_2\text{C}_3$) phase after etching. After all these experimental studies, the products were characterized by XRD, SEM and TEM analysis. Their electrochemical performances were investigated by cyclic voltammetry (CV) and galvanostatic charge-discharge (GCD) measurements. According to the characterization results, it was understood that acicular MnO_2 crystals with a thickness of less than 50 nm and a length of more than 100 nm were successfully synthesized together with MXene on the carbon fabric surfaces. In terms of electrochemistry, it was observed that the performance increased as the MXene contribution increased, and the highest performance was observed in the sample with 15 mg MXene added. The specific capacitance of this sample was approximately 1100 mF/cm^2 , while the energy and power densities were determined as 72 mWh/cm^2 and 230 mW/cm^2 , respectively. It is thought that these results make a significant contribution to the literature with a very high performance.

Key Words: Mxene ($\text{Ti}_3\text{C}_2\text{T}_x$), MAX, ($\text{Ti}_3\text{Al}_2\text{C}_3$), MnO_2 nanorod, flexible supercapacitor.

Science Code : 91520, 91530

ÖZET

Yüksek Lisans Tezi

MnO₂@Ti₃C₂T_x KATKILI KARBON KUMAŞ ESASLI ESNEK SÜPER KAPASİTÖR ELEKTROTLARININ HAZIRLANMASI

Karabük Üniversitesi

Fen Bilimleri Enstitüsü

Metalurji ve Malzeme Mühendisliği Anabilim Dalı

Mariem ABDI

Tez Danışmanı:

Doç. Dr. Safa POLAT

Ocak 2023, 60 sayfa

Küresel nüfusun artışıyla birlikte yenilenebilir enerji kaynaklarının geliştirilmesine yönelik yapılan araştırmaların artışıyla birlikte enerji depolama sistemlerine (EDS) olan talepte de önemli bir artış meydana gelmiştir. Özellikle son yıllarda geliştirilen esnek yapılı robotlar, biyo sensörler ve yeni nesil esnek ekranlı cep telefonları gibi tüketici elektroniği ihtiyacını karşılayabilmek amacıyla esnek yapılı EDS'lere ihtiyaç duyulduğu bilinmektedir. Süperkapasitörler bu bakımdan kullanılan ve geliştirilmekte olan en yaygın EDS'lerden birisidir. Bu çalışmada esnek yapılı süper kapasitörler için karbon kumaş bazlı MnO₂@MXene katkılı kompozit elektrotların üretimi amaçlanmıştır. Bu amaçla akım toplayıcı iletken ve esnek karbon kumaşlar kullanılmıştır. Bunlar pamuklu kumaşın oksijensiz ortamda yüksek sıcaklığa maruz bırakılması ile elde edilmiştir. Daha sonra bu kumaşların yüzeylerini fonksiyonel hale getirmek için hidrotermal yöntemle MnO₂ sentezlenmiştir. Ayrıca bu sentezlere farklı oranlarda MXene katkıları da yapılmıştır. MXene yapısı ise MAX (Ti₃Al₂C₃) fazından

etching sonrası alüminyumun uzaklaştırılması ile sağlanmıştır. Tüm bu deneysel çalışmaların ardından ürünler XRD, SEM ve TEM analizleri ile karakterize edilmiştir. Elektrokimyasal performansları ise çevrimli voltametri (CV) ve galvano statik şarj deşarj (GCD) ölçümleri ile incelenmiştir. Karakterizasyon sonuçlarına göre karbon kumaş yüzeylerinde yaklaşık 50 nm'den daha küçük kalınlıkta ve 100 nm'den daha uzun boyda iğnemsî MnO₂ kristallerinin MXene ile birlikte başarılı bir şekilde sentezlendiği anlaşılmıştır. Elektrokimyasal bakımından ise MXene katkısı arttıkça performansın da arttığı ve en yüksek performansın ise 15 mg MXene katkılı olan numunenin olduğu gözlenmiştir. Bu numunenin spesifik kapasitansı yaklaşık 1100 mF/cm² iken enerji ve güç yoğunlukları da sırasıyla 72 mWh/cm² ve 230 mW/cm² olarak tespit edilmiştir. Bu sonuçların oldukça yüksek bir performans ile literatüre önemli katkı sağladığı düşünülmektedir.

Anahtar Kelimeler : Mxene (Ti₃C₂T_x), MAX, (Ti₃Al₂C₃), MnO₂ nanoçubuk, esnek süperkapasitör.

Bilim Kodu : 902.2.042

KNOWLEDGMENT

First and foremost praises and thanks to god for the blessings he gave me during my research.

I would like to acknowledge and give my warmest thanks to my supervisor Assist. Prof. Dr. Safa POLAT who made this work possible. His guidance and advice carried me through all the stages of my project.

Also I would like to express my gratitude to my colleagues Mariem MOHAMED EL MAMY, Muwafaq MASHRAH, Dana FARES, El Moctar MBEBOU, and Cheikh Sidi Mohamed LEFDHIL for their help during my experimental work. Their information has helped me complete this thesis.

I am extremely grateful to my family for their love, prayer, caring and continuing support to complete this research work. Also I express my thanks to the most important person in my life my father, Idoumou ABDI for his sacrifices for educating and preparing me for my future.

In addition I would like to thank the laboratories of Karabuk University Iron and Steel Institute Materials Research and Development Center (MARGEM) for allowing me to use the laboratory facilities.

Moreover I would like to thank the project numbered KBÜBAP-21-ABP-047 of Karabuk University Scientific Research Projects Unit (KBU-BAP), which provided funding for the analyses. This study was also supported by the Scientific and Technical Research Council of Turkey (TUBITAK) number 221M749. Thank you for the funding support.

CONTENTS

	<u>Page</u>
APPROVAL	ii
ABSTRACT	iv
ÖZET	vi
CKNOWLEDGMENT.....	viii
CONTENTS	ix
LIST OF FIGURES	xi
LIST OF TABLES.....	xii
SYMBOLS AND ABBREVIATIONS INDEX.....	xiii
PART 1.....	1
INTRODUCTION	1
1.1. MANGAN OXIDE AND MXENE PROPERTIES	5
1.1.1. Structure of MnO ₂	5
1.1.2. Electrochemical properties of MnO ₂	7
1.1.3. Ti ₃ C ₂ T _x production and its structure	8
1.1.4. Electrochemical properties of Ti ₃ C ₂ T _x	12
1.2. NANOPARTICLE SYNTHESIS AND ENERGY STORAGE FEATURES	13
1.2.1. Nanoparticles synthesize methods	13
1.2.2. Energy storage systems and supercapacitors	18
1.2.3. Characterization of supercapacitor electrodes	20
PART 2.....	22
LITERATURE REVIEW.....	22
2.1. SUMMARY OF PREVIOUS STUDIES.....	22
2.2.1. MnO ₂ based supercapacitor electrodes	22
2.2.2. Ti ₃ C ₂ T _x based supercapacitor electrodes.....	24
2.2. THE OBJECTIVE OF THIS STUDY	26

	<u>Page</u>
PART 3.....	28
EXPERIMENTAL PROCEDURE.....	28
3.1. MATERIALS AND METHODS	28
3.1.1. Carbon fabric production.....	28
3.1.3. MnO ₂ @Ti ₃ C ₂ T _x synthesis on CC surfaces	30
3.1. MATERIAL CHARACTERIZATION	32
3.2. ELECTROCHEMICAL CHARACTERIZATION.....	32
 PART 4.....	 36
EXPERIMENTAL RESULTS AND DISCUSSION	36
4.1. MATERIALS CHARACTERIZATION RESULTS	36
4.2. ELECTROCHEMICAL MEASUREMENT RESULTS.....	40
 PART 5.....	 47
SUMMARY	47
REFERENCES	48
RESUME.....	60

LIST OF FIGURES

	<u>Page</u>
Figure 1.1. Structure and formula of manganese dioxide [45].....	6
Figure 1.2. Crystal structures of MnO ₂ polymorphs [46].....	6
Figure 1.3. The basic structure of MAX and the corresponding MXenes [61].....	9
Figure 1.4. Representation from MAX to Mxene conversion [64].	10
Figure 1.5. Schematic of porous electrode materials used in a supercapacitor [103].	20
Figure 3.1. Chalcopyrite unit cell (Cu: red, Fe: blue and S: yellow color).....	29
Figure 3.2. Production stages by hydrothermal method	29
Figure 3.3. Production stages by hydrothermal method	31
Figure 3.4. Digital image of carbon fabrics before and after synthesis	31
Figure 4.1. XRD analysis of MAX phase to MXene conversion	37
Figure 4.2. XRD analysis results of products after MnO ₂ synthesis	37
Figure 4.3. SEM images of a-b) carbon cloth, c-d) Mxene and MnO ₂ doped carbon cloth and e-f) TEM image of MXene and MnO ₂ doped carbon fabrics.	39
Figure 4.4. CV curves of M1 sample	40
Figure 4.5. CV curves of M2 sample	41
Figure 4.6. CV curves of M3 sample	41
Figure 4.7. GCD curves of M2 sample	43
Figure 4.8. GCD curves of M2 sample	43
Figure 4.9. GCD curves of M3 sample	44
Figure 4.10. Specific capacitance values of electrodes.....	45
Figure 4.11. Energy and power density of electrodes.....	46

LIST OF TABLES

	<u>Page</u>
Table 3.1. Production parameters.	31

SYMBOLS AND ABBREVIATIONS INDEX

SYMBOLS

A	: Ampere
mA	: Milliampere
g	: Gram
mg	: Milligram
°C	: Degrees Celsius
s	: Second
KMnO ₄	: Potassium Permanganate
mF	: Millifarad
mWh/cm ²	: Milliwatts hour per centimeter squared
mW/cm ²	: Milliwatts per centimeter squared
MnO ₂	: Manganese dioxide
Ti ₃ AlC ₂	: Maxphase
Ti ₃ C ₂ T _x	: Mxene

ABBREVIATIONS

Cs	: Specific capacitance
E	: Energy density
P	: Power density
SEM	: Scanning Electron Microscope
TEM	: Transmission Electron Microscope
XRD	: X-Ray Diffraction
CV	: Cyclic Voltammetry
GCD	: Galvanostatic charge-discharge

PART 1

INTRODUCTION

With the increase in research on the development of renewable energy sources, there has been a significant increase in the demand for energy storage systems (EDS) [1–4]. EDSs generally refer to devices used to convert electrical energy from power systems back into electrical energy when necessary [5]. It is known that flexible EDSs are needed in order to meet the needs of consumer electronics such as flexible robots, biosensors and new generation mobile phones with flexible screens, which have been developed in recent years [6]. In addition, it is known that flexible EDSs are needed for wearable triboelectric nanogenerators developed for electricity generation from daily activities [7]. Supercapacitors are one of the most common EDS used and under development in this regard.

Supercapacitors are generally categorized into two classes as electrochemical double capacitors (EDLCs) and pseudocapacitors (PC) when viewed from charge storage controls [8]. EDLCs store energy electrostatically via surface ion adsorption/desorption at electrodes/electrolyte interfaces, while PCs use fast and reversible surface Faradic responses between emission ions and electroactive materials. The specific capacitance (SC) of EDLC is directly proportional to the surface area of the electrode material accessible to the electrolyte ions [9]. Therefore, porous carbon materials (e.g. activated carbon or graphene) with a large specific surface area (500–3000 m²/g) are widely used as commercial electrode material [10]. However, EDLCs suffer from relatively low specific capacitance and limited energy density (normally <10 W h/kg). The specific capacitance of PCs exceeds that of EDLCs due to redox reactions, where more charge can be stored in capacitor systems [11–14]. Transition metal oxides and conductive polymers are typically used in this context as electroactive electrode materials for PCs. The military application of RuO₂ is one of the most successful

examples of this, due to its high specific capacitance of about 600 F/g [15]. However, RuO₂'s high cost and toxicity issues limit its widespread application. Therefore, many studies are carried out to develop inexpensive and environmentally friendly alternatives such as MnO₂, Fe₃O₄, Co₃O₄ and NiO [6,16,17].

Among these metal oxides, MnO₂ is one of the promising electrode materials due to its abundance in nature, low cost, environmental friendliness and high theoretical specific capacitance (SC) (1370 F/g) [18]. It has been stated that MnO₂ has a wider electrochemical potential range of approximately 0.9–1.0 V in an aqueous electrolyte compared to Co₃O₄ and NiO (0.4–0.5 V) [19,20]. It also has the important advantage of being able to use soft aqueous electrolytes, which cause much less chemical corrosion in current collectors. However, due to the wide band gap (~2.68 eV), MnO₂ electrodes also have important disadvantages such as poor conductivity (10⁻⁵-10⁻⁶ S/cm) [21], low ionic diffusion constant (~10–13 cm²/Vs) and easy aggregation, which may cause a decrease in electrochemical performance. In their use as super capacitors, problems such as poor cycle stability, low electrical conductivity and large volume expansion/contraction during charge-discharge process arise due to such disadvantages. However, it was stated that this problem was directly related to electron and ion transfer, and it was thought that MnO₂ could be solved by both expanding the surface area and increasing its electrical conductivity. For this reason, it has been stated that the studies in the literature should focus on the synthesis of MnO₂ at nanoscale [22]. For example, Zhang et al. have synthesized MnO₂ in the form of nano dendrites by electro storage method and determined the specific capacitance of the electrodes at 1 A/g current density as 469 F/g [23]. Goma Ali et al. synthesized the nanoflower product MnO₂ and kept the specific capacitance value of 309 F/g [24]. Grote et al., on the other hand, determined the specific capacitance values of the MnO₂ electrodes they produced in nanotube and nanowire form as 210 F/g at 1.9 A/g current density and 231 F/g at 0.5 A/g current density, respectively [25]. He et al., on the other hand, found that the specific capacitance value was 336 F/g when they synthesized MnO₂ in the form of nanoflake with the nanotube edges in the middle on the graphene foam surface [26]. It can be said that the capacitance values are significantly increased by synthesizing MnO₂ crystals in the aforementioned geometries and in nano size. It is also stated that these structures, especially those with nanotube geometry, have a

significant advantage due to their thin walls and large surface area that allow diffusion [27,28]. However, due to the low conductivity of MnO_2 , the capacitance value is still very low compared to the theoretical one (1370 F/g). In addition, it has been stated that the use of polymeric binders to hold such nanostructures on the current collector reduces the surface area and negatively affects the capacitance [29]. Therefore, it has been proposed to directly synthesize MnO_2 on current collector surfaces. It has been stated that the synthesis of metal oxides in the aforementioned geometries on the carbon cloth-like substrate surface using the hydrothermal method is a very effective and proven method [30]. On the other hand, even though the surface area is expanded by producing MnO_2 's in the aforementioned geometries, electron exchange is still poor due to its low conductivity, and it has been suggested that conductivity-enhancing secondary components can be used to increase the capacitance. In order to increase conductivity, it has been stated that it is used with 1D and 2D components such as graphene and carbon nanotubes in many studies, but aggregation caused by π - π interactions is an important problem (S.-Y. Yang et al., 2011). Therefore, MXene structures composed of transition metal carbides or carbonitrides have emerged as an alternative to carbon-based two-dimensional components [31]. These structures are obtained by chemical etching of the MAX phase synthesized at high temperature and pressure with acids such as HF and HCl. During etching, element A (usually composed of IIIA and VIA group elements) goes into solution and a hydrophilic group is attached to the outer part of the M-X structure, ending the structure. In these structures with the chemical formula $\text{M}_{n+1}\text{X}_n\text{T}_x$, M represents the transition metal, X represents carbon or nitrogen atoms, n represents an integer between 1 and 3, and T represents functional groups such as oxygen, hydroxyl or fluorine [23]. The fact that the outer parts of these structures consist of a functional group causes them to have very high electrical conductivity (1000 Scm^{-1}) [20,32]. In addition, when the A layer passes into the solution, it causes the formation of leaf-shaped stratified cavities in the structure, which ensures that MXene structures have a two-dimensional large surface area [33]. In this context, approximately 70 different MXene structures have been synthesized in studies conducted so far [34], and it has been stated that the most widely used one is $\text{Ti}_3\text{C}_2\text{T}_x$ [23,35]. At the same time, $\text{Ti}_3\text{C}_2\text{T}_x$ structure provides fast electron feeding to the electrochemically active sites due to having a conductive inner transition metal carbide layer. In addition, the hydroxyl sites forming the outer structure of MXene are

very active against redox reactions. Due to these properties, it has become a very interesting component in the field of energy storage in the last few years. However, in studies conducted for this purpose, it has been stated that the theoretical capacitance value of an undoped $Ti_3C_2T_x$ structure is maximum 615 C/g, and in experimental studies, these values are around 245 F/g to 135 C/g [35,36]. On the other hand, in another study, it was suggested that this difference observed between the theoretical and experimental results of the $Ti_3C_2T_x$ component could actually be reduced by appropriate cation interaction of its layers and appropriate surface modifications [37]. This recommendation has made $Ti_3C_2T_x$ an important component for metal oxides such as MnO_2 , which have poor electrical conductivity but are capable of rapid redox reaction. For this purpose, Wu et al. determined the capacitance value of the electrodes they prepared as 511 F/g, the energy density as 29.58 Wh/kg and the power density as 750 W/kg by performing MnO_2 synthesis together with $Ti_3C_2T_x$ on the carbon fabric surface [38]. They also stated that the capacitance values of the electrodes decreased by only 17% after 10000 cycles. These studies generally show that the capacitance value of both MnO_2 and $Ti_3C_2T_x$ increases up to a certain level as a result of the interaction of MnO_2 with the MXene structure. Based on these very promising results, a carbon fabric-based flexible supercapacitor with $MnO_2@Ti_3C_2T_x$ can be designed. In such a design, it is thought that both the conductivity and the expansion of the surface area can be achieved by the synthesis of MnO_2 crystals in nanotube form (MNT) and $Ti_3C_2T_x$ interfaces, as suggested in the literature, and thus very high capacitance values can be achieved. However, both the relationship of MnO_2 with $Ti_3C_2T_x$ structure and the synthesis of these components on flexible carbon fabric surfaces are quite new, and in this respect, some deficiencies that have not been examined in the literature have been observed [23,39]. These are itemized below.

It is an important deficiency that MnO_2 and $Ti_3C_2T_x$ components are not synthesized on carbon fabric surfaces at different concentrations. The effects of both components together, but in different amounts, need to be examined synergistically. For this reason, it was aimed to produce MnO_2 and Mxene doped carbon cloth-based electrode by changing amount of Mxene in the electrode. In order to carry out of this purpose, these electrodes were produce by hydrothermal method. After that, the electrodes were characterized by XRD, FTIR, SEM and TEM analysis. Then, the electrochemical properties of it's were performed by cyclic voltammetry (CV) and galvanostatic charge

discharge (GCD). All the obtained results were then discussed by comparing in literature.

1.1. MANGAN OXIDE AND MXENE PROPERTIES

1.1.1. Structure of MnO₂

Manganese dioxide (MnO₂) has gained a lot of attention in the last 10 years due to its unique physical and chemical characteristics and wide range of applications in catalysis, ion exchange, molecular adsorption, biosensors, and energy storage [40]. MnO₂ in particular has been identified as a viable electrode material for supercapacitors due to its low cost, environmental friendliness, and outstanding capacitive performance in aqueous electrolytes [41].

As a result of the varied bonding patterns of MnO₆ bipyramids, MnO₂ shows many structural polymorphs such as hollandite (α), pyrolusite (β), intergrowth (γ), birnessite (δ), Ramsdellite (R-MnO₂) and defect spinel (λ) as seen in figure 1.1 and figure 1.2 [42,43]. The Polymorphs have different atomic configurations, resulting in different sorts of pores or tunnels inside the crystal structure. The selectivity towards various ions or electron transfer kinetics is enormous due to the particular crystal structure. Because the majority of electrical energy storage system (EESS) employs ions in the electrolyte and electron transfer kinetics on the electrode surface, it is assumed that the crystal structures and applications are closely connected [44].

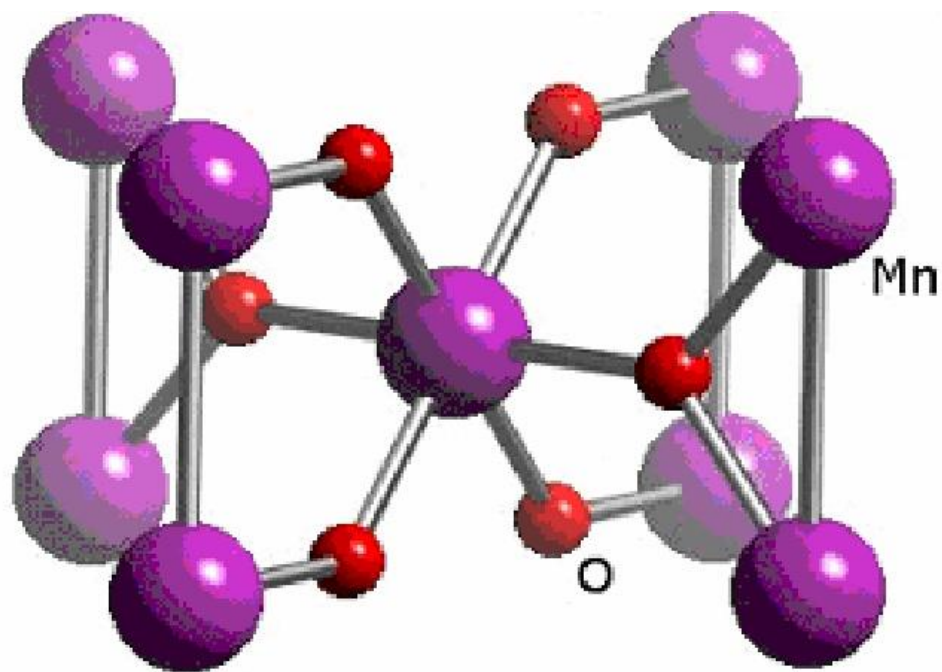


Figure 1.1. Structure and formula of manganese dioxide [45].

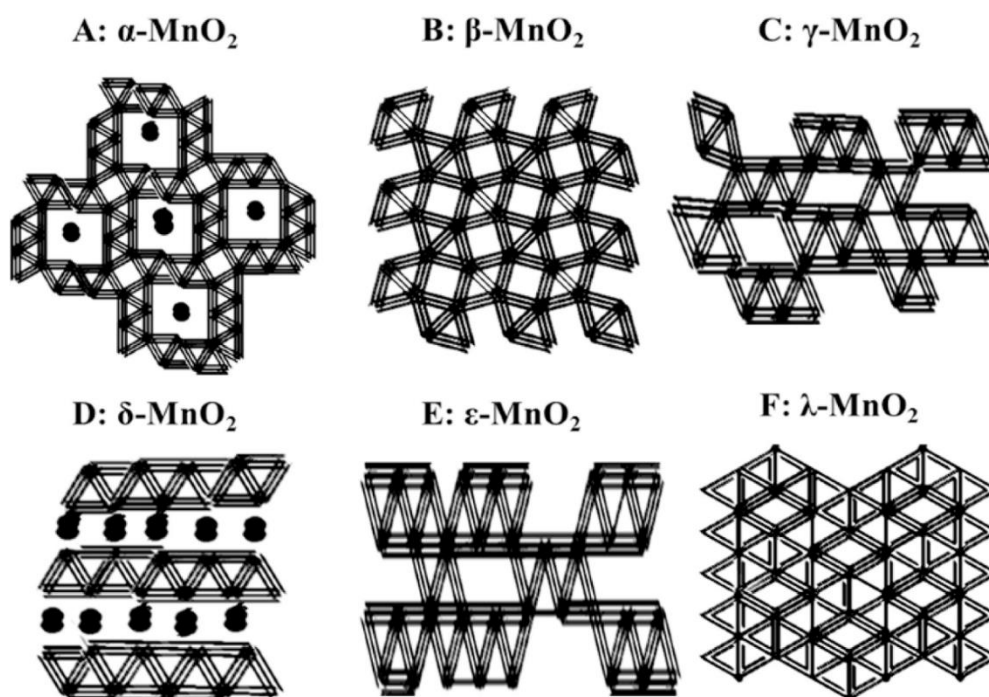


Figure 1.2. Crystal structures of MnO₂ polymorphs [46].

The crystal phase is a key element in determining MnO₂ activity, however varied results were obtained from different reaction systems. Zhao et al. discovered that urchin-like γ -MnO₂ was more active in NO oxidation than α -, β - and δ -phase MnO₂,

and that more active oxygen species on the surface of disordered γ - MnO_2 were responsible for its superior performance [47]. Al_2O_3 supported α - MnO_2 outperformed supported β - MnO_2 and γ - MnO_2 , which is due in part to the higher oxygen mobility and higher adsorption of VOCs [48]. In a comparative investigation of oxidation over α , δ -, γ - and β - MnO_2 , Liang et al. found that the oxidation activity of catalysts declined in the order of α - $\text{MnO}_2 \approx \delta$ - $\text{MnO}_2 > \gamma$ - $\text{MnO}_2 > \beta$ - MnO_2 [49]. Similarly, in the activation of Oxone to form sulfate radicals for phenol degradation, α - MnO_2 , γ - MnO_2 and β - MnO_2 were studied, and an equivalent order of α - $\text{MnO}_2 > \gamma$ - $\text{MnO}_2 > \beta$ - MnO_2 of catalytic activity was reported here [50]. Manganese dioxide is a common electrode material in dry cell batteries like alkaline and Zn-Cd batteries. Manganese dioxide was also utilized in 1976 as a material for super capacitor electrodes [51]. MnO_2 is also employed as a catalyst in the synthesis of oxygen from potassium chlorate [52].

1.1.2. Electrochemical properties of MnO_2

The electrochemical characteristics of nano-structured MnO_2 are heavily impacted by nanoparticle dimensions, sample shape, composition, and production. As a result of its outstanding electrical capabilities, many morphologies of lower dimensional space nanostructured MnO_2 have been created, including rods, belts, wires, ribbons, and tubes and subsequently, the utilization of innovative multilevel nano-structured MnO_2 as a lithium-ion inclusion host was already described [53]. Sunaina et al. used a simple hydrothermal approach to create one-dimensional α - MnO_2 nanostructures with different morphologies by altering the hydrothermal temperature. The XRD and Raman spectroscopy confirmed the tetragonal α - MnO_2 phase. FESEM study revealed morphological variability from nanorods to nanofibers. The super capacitive characteristics of the produced electrode material were investigated utilizing electrochemical characterizations such as CV and GCD. In this situation, the nanorods collected to form a spherical shape exceeded the nanofibers generated at a higher temperature in terms of electrochemical performance. As a result, the hydrothermally produced α - MnO_2 nanostructures might be recognized as an important electrode choice for high-performance supercapacitors [49]. Teli et al. synthesized the MnO_2 under high temperatures. They stated that this condition leads to a change in the morphology and crystalline structures of their samples, so the specific capacitance was

directly affected, and 300°C was the best temperature with the highest specific capacitance and the highest stability in aqueous electrolyte. So the samples are the most suitable in these conditions for the measurement [54]. By a simple hydrothermal method, Chen et al. prepared MnO₂ nanorods from KMnO₄ and HCl. MnO₂ nanorods have dramatically improved electrochemical performance, including high capacity, great cycle stability, and outstanding rate capability. An initial reversible capacity of 1206.1 mAhg⁻¹ is attained, with an initial coulombic efficiency of 74.9%. The reversible capacity of 1404.7 mAh g⁻¹ is maintained after 100 cycles at varied c-rates. The good electrochemical characteristics are due to the unique structure of MnO₂ nanorods and the use of CMC binder. MnO₂ nanorod is a potential anode material for next-generation lithium ion batteries, according to the findings [43].

1.1.3. Ti₃C₂T_x production and its structure

Two-dimensional (2D) materials have become a main research interest in materials science since the discovery of graphene and its remarkable properties [55]. Because of their unique physicochemical characteristics, diverse two-dimensional (2D) materials have been extensively researched [56]. Due to their large surface-area-to-volume ratio and interior surface areas, 2D materials provide great mobility and energy density, which make them ideal candidates for energy storage devices [56]. A novel family of 2D materials known as MXene has just evolved, consisting of transition metal carbides, nitrides, and carbonitrides [57]. These new materials are obtained by selectively etching out the A layers from their respective three-dimensional (3D) MAX phases [58], with a general formula of M_{n+1}AX_n (n = 1, 2 or 3) consisting of early transition metal “M”, main group element “A”, and carbon and/or nitrogen “X” [59]. MAX/M_{n+1}AX_n may be classified into three varieties based on the value of n (n = 1, 2, 3). These include M₂AX₁ (211), M₃AX₂ (312), and M₄AX₃ (413) [60]. In a typical crystal structure of a layered MAX/M_{n+1}AX_n phase as shown in Figure 1.3.

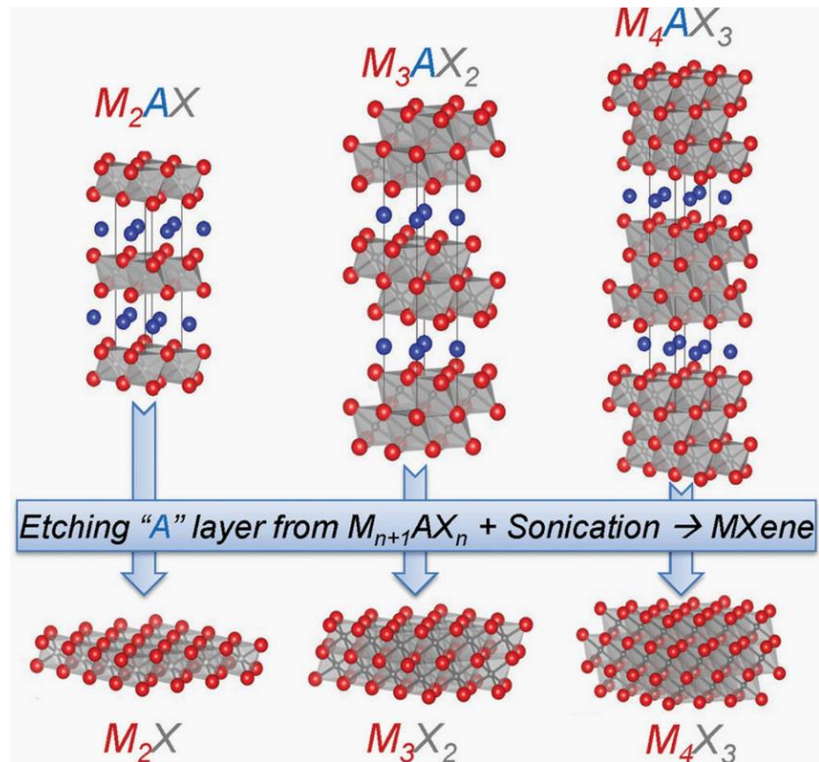


Figure 1.3. The basic structure of MAX and the corresponding MXenes [61].

More than 70 MAX phases have been detected to date [62], Furthermore, MAX phases may be created by combining solid solutions of "M", "A" and "X", such as $(Ti,Nb)_2AlC$, $Ti_3(A_{10.5}Si_{0.5})C_2$, and $Ti_2Al(C_{0.5}N_{0.5})$ [63]. The "A"-containing bonds are more chemically active than the strong M-X bonds. Thus, it is feasible to selectively etch "A" layers from the 3D MAX phase, resulting in a novel class of 2D graphene-like materials known as MXene. As previously stated, MXenes are typically produced by selectively etching A layers from their corresponding MAX phases at room temperature using aqueous HF as the etchant as shown in Figure 1.4.

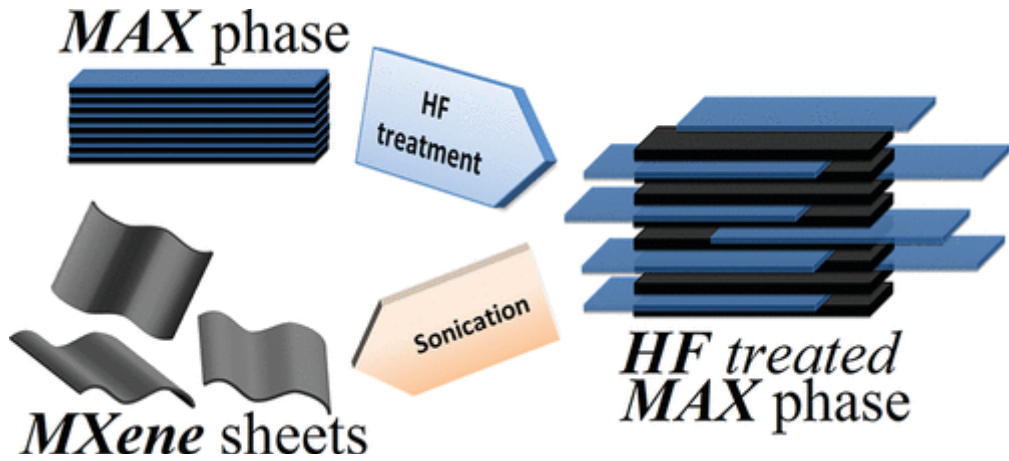


Figure 1.4. Representation from MAX to Mxene conversion [64].

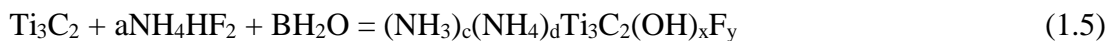
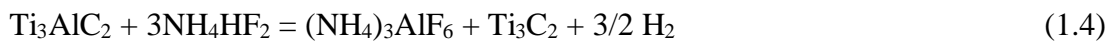
$Ti_3C_2T_x$ ($T = OH$ and F) was synthesized in the first experiment by removing the weakly bonded Al layers from the Ti_3AlC_2 phase [65]. The following equation 1.1, 1.2, 1.3 are the reactions of HF solutions with Ti_3AlC_2 :



The first Reaction (1.1) is the mandatory, (1.2) and (1.3) provide OH and F terminations, respectively. After that, centrifugation was used to separate the particles, which were then rinsed with deionized water. MXenes have multilayered structures without delamination. Sonication was used to create single- or few-layer MXenes, but it was eventually supplanted by dimethyl sulfoxide (DMSO) intercalation, which proved to be more effective [66]. Almost all other MXene sheets were prepared using this approach from Al-containing MAX phases. Notably, depending on particle size and temperature, the etching conditions (time and HF concentration) required to convert a particular MAX phase vary greatly. For example, attrition or ball milling can effectively reduce the required etching time and/or HF concentration by lowering the MAX phase particle size. Furthermore, differences in M-Al bond energies for various MAX phases need distinct etching conditions. For example, the higher Ti-Al bond

energy in Ti_2AlC compared to Nb_2AlC resulted in a longer etching time and higher HF concentration [67].

Recently, a trend of searching for an alternative for HF etchant prompted the research of several new synthesis procedures since HF is toxic to the body, making handling the chemical difficult, and it may also release harmful wastes that have an impact on the environment. Attempts were made to find softer etchants with less waste and toxicity. Halim et al. demonstrated that Ammonium Bifluoride (NH_4HF_2) is a viable choice. Initially, epitaxial Ti_3AlC_2 thin films were formed on sapphire substrates at 780 °C, according to the study. Then, a comparison study was performed, the first with traditional 50% concentrated HF on samples with thicknesses of 15, 28, 43, and 60 nm for 10, 15, 60, and 160 minutes, respectively. In the second investigation, 1 M of NH_4HF_2 was utilized, with the sample thicknesses indicated before but for 150, 160, 420, and 660 min, respectively. This approach is a one-step synthesis method for MXenes since ammonia (cations) were intercalated simultaneously during the etching process, which is a significant benefit over HF etching [68]. Because the etching and intercalation processes occur concurrently, it is possible to expect the following reactions (equation 1.4 and 1.5):



Reaction (equation 1.5) demonstrates that NH_3 and NH_4^{+1} is intercalated between $Ti_3C_2T_x$ layers, altering MXene characteristics considerably. As the distance between the layers grows, the MXene swells (the c lattice parameter was raised by 25% compared to the films etched with HF). Because NH_4HF_2 is less toxic than HF, it is a gentler etchant. Ghidiu et al. proposed a new high-yield process for the simultaneous fabrication of several MXene sheets [69]. In this method, $Ti_3C_2T_x$ was produced by dissolving Ti_3AlC_2 particles in LiF and HCl solutions, then heating the mixture at 40 °C for 45 hours, and lastly washing the sediment to remove the product and elevate the ph. This technique yielded a clay-like paste, which could be rolled to generate flexible, free-standing films with high volumetric capacitance. This was the first instance of the

comparable nature of MXenes, and clays being brought to light. In this situation, water intercalation acts as a lubricant, allowing for easy shearing, reducing the standard sonication time for delamination from 4 h to 30-60 min. Other fluoride salts, such as NaF, KF, CsF, and CaF₂, can be used in place of LiF in HCl or H₂SO₄.

1.1.4. Electrochemical properties of Ti₃C₂T_x

Naguib et al. discovered that Ti₃C₂T_x oxidizes in air, CO₂, and pressured water [70]. It was reported that the oxidation produced anatase TiO₂ nanocrystals encased in amorphous carbon sheets (TiO₂-C hybrid structure). It was anticipated that during flash oxidation, the top and bottom Ti layers oxidized to produce thin anatase nanoparticles; however, during slow oxidation, the top and bottom Ti layers oxidized to generate sheets of nanocrystalline rutile. As a result, two distinct TiO₂ phases were formed under the two different oxidation regimes. Similarly, Li et al. determined that Ti₃C₂T_x may react with O₂ to generate TiO₂ in either rutile or anatase phases [71]. In contrast to the TiO₂-C hybrid structure, the anatase nanocrystals generated were equally dispersed over the 2D Ti₃C₂ layers. The difference was caused by the prolonged reaction period of around 40 minutes compared to the <5 s flash oxidation; the newly generated carbon was unstable. The anatase phase would convert to rutile at high temperatures. A similar effect was described for Ti₂CT_x almost immediately [72]. Heat treatment produced anatase TiO₂, which later transformed to rutile TiO₂ at higher temperatures [27]. Lui et al. Found that by considering Ti₃C₂T_x MXene as a promising electrode material for electrochemical energy storage. However, due to its low specific capacitance concerns, its practical uses are limited. A simple heteroatom doping approach is presented in this paper to create defect-rich Ti₃C₂T_x MXene with numerous active sites. As a result, P-doped Ti₃C₂T_x MXene was produced using a simple annealing process. The synthesized P-doped Ti₃C₂T_x was employed as the SC electrode material, and it was discovered that the P-doped Ti₃C₂T_x displays improved electrochemical performance when compared to the pristine Ti₃C₂T_x MXene, with a high specific capacity of 31.11 mA h g⁻¹ at 1 A g⁻¹ in 1 M KOH electrolyte. Furthermore, a P-doped Ti₃C₂T_x-based symmetric SC device with an energy density of 8.2 Wh L⁻¹ and a power density of 303.4 W L⁻¹ is constructed [73]. Redox-enhanced electrochemical capacitors (redox ECs) are promising energy-storage devices with the

potential to deliver both high power and energy performances, but overcoming the severe self-discharge remains a significant challenge due to the shuttle effect of redox species such as I^-/I_3^- ions introduced in the electrolytes to gain additional capacities. Yang et al. suggest a cation-initiated self-assembly technique of $Ti_3C_2T_x$ MXene nanosheets onto glass fiber membranes to construct Janus separators that can reduce I^-/I_3^- ion shuttling in iodine-based redox ECs. Because various cations such as imidazolium (C_4mim^+), Mg^{2+} , and Al^{3+} may be used to regulate the interlayer spacing of the MXene films, the resultant Janus separators have customizable nanochannels for ion sieving. Both molecular dynamic (MD) simulations and electrochemical testing show that C_4mim^+ -intercalated MXene Janus separators (C_4mim^+ -MXene) may restrict I_3^- ion diffusion while permitting other electrolyte ions to pass. As a result, self-discharge caused by the shuttle effect can be significantly reduced in C_4mim^+ -MXene-based redox ECs, which deliver significantly higher voltage and energy retentions than glass fiber membrane separator-based cells (voltage retention: 70% vs. 10%, energy retention: 51% vs. 6.5%) after a 24-h open-circuit test [74]. Zhang et al. verified that the ultrasonic substantially aided the intercalation of Li^+ between the neighboring layers of $Ti_3C_2T_x$ MXene. Under the influence of ultrasound, the 8-hour sonicated etching demonstrated a specific capacitance of 270.5 F/g, a 16-fold increase over the control sample. They produced monolayered samples with and without sonication treatment, and the sample created with ultrasound had a specific capacitance of 420.66 F/g. After 10,000 cycles at 5 A/g, the specific capacitance retention of the 8 h ultrasonically etched multiple layered samples was 95.52%, which was 4.27% higher than the comparable value of the monolayered sample [75].

1.2. NANOPARTICLE SYNTHESIS AND ENERGY STORAGE FEATURES

1.2.1. Nanoparticles synthesis methods

Nanotechnology is the development of structures that have improved and/or completely new physical, chemical, and biological qualities. This is accomplished by working at the level of atoms and molecules (within the range of 1 to 100 nm in units per billion). The material properties and operational principles of the devices are, in general, based on standard modeling and theory (assumptions based on dimensions

bigger than 100 nm). This is due to the fact that traditional modeling and theoretical frameworks are the representations of the physical world that are the most precise. Dimensions of its are generally smaller than 100 nanometers [76].

However, render existing theories and models are inadequate for describing the newly manifesting features. In comparison to bigger particles of the same substance, nanomaterials exhibit superior and distinctive properties due to their diminutive size. One may find a wide variety of nanomaterial's and particles on Earth in their unaltered, native forms. Exhaust gases, volcanic byproducts, and photochemical chemicals are all examples of such substances [77].

The fundamental goal of nanotechnology is to pave the way for the development of goods that are more robust, of better quality, last longer, are less expensive, lighter, and smaller in size. Several nanoscale manufacturing technologies are now in development as a result of this impetus. These topics will be covered in further detail in the next paragraph. Subheadings also include topics like the characterization of nanoparticles and their use in supercapacitors for this specific application. Nanomaterials and nanostructures may be manufactured using one of two main approaches: top-down production or bottom-up production. The first approach, which is known as the Top-down technique, starts with the whole information, which is then divided into digestible portions once the operation has been carried out. The “bottom-up” technique is another name for this approach to problem solving. This fundamental approach reduces the structural dimensions of microscopic components down to the nanoscale scale by using lithography, incredibly flawless surface shaping, particular processing procedures, and chemical etching methods. The bottom-up production approach includes the synthesis of the material as a result of the growth in size of atoms and molecules brought about by chemical processes. This development in size takes place throughout the manufacturing process. Atomic and molecular components are brought together in a manner that is under regulated circumstances in order to generate larger systems, clusters, organic lattices, multimolecular structures, and synthetic macromolecules. This process takes place in a controlled environment. These may be divided up into the following three categories: Synthetic processes that may be carried out in solid phase, liquid phase, or gas phase environments [36,37]. The inert gas

condensation technique is one of the most favored ways for manufacturing nanoparticles due to its ability to provide flexibility and controlled material synthesis [79]. The two processes that comprise the method's main working principle are evaporating the starting material in the presence of a pure helium atmosphere and then cooling the vapor that is formed in the presence of the helium atmosphere [80]. Following this process, the condensation of atoms into micro particles occurs. The nano particles produced as a result of this action are subsequently transported and collected in the collector. Convection currents move small, condensed particles into the collecting jar, which are heated by the inert gas and cooled by the cold finger. The sediments are scraped and then transported to the compression equipment. The particles generated range in size from one to one hundred nanometers, and the size of the particles produced may be varied by varying the gas pressure. The obtained particles might then be sintered to generate solid nanomaterials if that is needed. The primary factors affecting the system and product characteristics are the gas pressure, inert gas type, temperature, and gas flow rate [81].

Physical vapor deposition (PVD) is a coating technology that uses vapor convection and condensation to coat material from a solid or liquid source (typically in a vacuum environment) [82]. This method may generate thin films with dimensions as small as an atom or as large as a nanometer as long as the manufacturing conditions are rigorously maintained. This is a versatile production technology. Evaporation, sputtering, laser heating, and ion beam are all examples of vapor phase types produced by the PVD process [83]. Atoms are separated from the surface of the target by the impact of ions in sputtering, but atoms are removed from the source via thermal techniques in evaporation. After the resulting vapor phase has gone through the collision and ionization stages, the substrate begins to concentrate on the sample, which is subsequently followed by the nucleation and growth processes. Sputtering is also used to create layers of materials with high melting temperatures, such as refractory metals and ceramics, which are difficult to produce by thermal evaporation. These layers can then be used in a variety of ways. Sputter-formed films have a higher density than evaporation-formed films because sputtering atoms carry more energy than evaporating atoms. Two of the key advantages of adopting these technologies are

their ability to make thick films at extremely low substrate temperatures and their quick film growth rates [84].

In 1994 in Germany where the first invention of the chemical vapor deposition (CVC) method as an excellent method for producing large quantities of nanoparticles [85]. Thermal cracking transforms gaseous material into particles in this technique. This is the procedure's essential concept. Chemical vapor deposition (CVD) is a common manufacturing method at the nanoscale. Its principal role is to coat the surface with a thin film, but it is also used in the production of high-purity bulk materials and powders [86]. Gaseous or vaporous raw materials are deposited onto the heated substrate during the CVD process, where they either react chemically or serve as a transport medium for additional raw materials. Reactions occur on or near hot surfaces, and the ensuing solid products are deposited on the surface as thin films. It is possible to make a wide range of various materials using this method. The CVD process employs several different types of reactors. They are classified as having hot or cold walls, being low pressure, atmospheric pressure, or high pressure, and having or not having carrier gas. Deposition techniques may be carried out inside these reactors at temperatures ranging from 473 to 1873 K. At the same time, chemical vapor deposition (CVD) procedures may be divided into many groups based on the kind of energy source employed (plasma, photon, laser, or hot filament). The CVD technique has several advantages. One of the most notable advantages of the method is that it can frequently generate a homogeneous thick film or coating layer on elaborately formed components. Another of the CVD technique's numerous advantages is its potential to ease the synthesis of materials with extremely high purity. Other advantages include relatively high deposition rates and a general requirement for a vacuum that is frequently lower than that required for PVD processes within these reactors [86]. The particle formation method in liquid phase synthesis is identical to that in vapor phase synthesis. Although grain size and crystal shape are difficult to regulate in standard gas condensation, they can be controlled in sol-gel and solvothermal synthesis by using growth-limiting organic ligands. During chemical precipitation (CP) reactions, the processes of nucleation, growth, and/or agglomeration may all occur concurrently. Supersaturation conditions are frequently required for the production of insoluble particles. The nucleation stage is the most crucial since it produces a large number of minute

particles. Secondary processes, on the other hand, such as maturation or aggregation, have a significant influence on the final product's size, form, and features after they have been finished [87]. It is important to obtain supersaturation (saturation), which commonly occurs as a result of a chemical reaction, in order to facilitate the precipitation process. Metal synthesis (from aqueous solutions, reduction from non-aqueous solutions, electrochemical reduction, and degradation of metal-organic precursors) and oxides (from both aqueous and non-aqueous solutions) are examples of common chemical precipitation processes (by molecular precursor reactions). Chemical precipitation procedures utilizing microwaves and sonication may also be applied [88].

Another wet-chemical process is the sol-gel method. A network structure known as a gel is created during this method by using either a chemical solution known as a solvent solution or colloidal particles known as a sol for nanoscale particles [89]. The technique begins with the creation of a stable sol containing solid particles in solution, followed by either a polycondensation or a sol-gel reaction. The gel's former liquid phase is removed by drying it. A high temperature is utilized at the end of the operation to densify and breakdown the gels. During this period, the gel precipitates in the network structure as pores, and any leftover organic contaminants are removed [90]. Gel is the interphase connected network, whereas sol is a colloidal dispersion of solid particles in a liquid phase. Sol can be considered a kind of gel. Instead of creating particulate metallic sols, both techniques produce polymeric sols (free of oxide particles larger than 1 nm). Both of these reactions are multi-step processes that occur in the specified order. Metal alkoxides, as well as inorganic and organic salts, can be used as precursors for sol-gel materials. Metal alkoxide precursors (Si, Ti, Zr, Al, and B) are used in a wide range of studies [91].

Hydrothermal synthesis is regarded as one of the most efficient methods for producing pure metal oxide nanoparticles. This approach allows for the formation of compounds that are insoluble under normal temperature and pressure settings by exploiting a heterogeneous reaction at high temperatures and pressure. The process of producing crystals takes place in an autoclave, which is a steel pressure vessel. The water and nutrients are maintained separate inside this gadget. Hydrothermal synthesis allows for

the creation of materials that would not be possible by solid-state processes. Following this process, you will get the final product, which has a low melting point, a high vapor pressure, and thermal breakdown. It is straightforward to create commodities in the intermediate, meta-stable, and certain phases, and it is also feasible to synthesize new meta-stable state chemicals and other substances in specific condensed states. The most notable disadvantages of hydrothermal synthesis include the requirement for pricey autoclaves, the existence of possible safety hazards throughout the reaction process, and the lack of any methods of seeing the reaction [92]. The process of grinding by use of technology the "top-down" approach to the synthesis of nanomaterials is shown by the method of mechanical etching, which is an excellent illustration of how this strategy works. This method uses plastic deformation to structurally deteriorate coarse particles to make nanomaterials [93]. Mechanical grinding of materials is widespread because it is simple, requires no expensive apparatus, and produces materials of numerous grades, including nanocrystalline materials. In reality, contamination from the grinding environment and consolidation of the powder result into a nanocrystalline microstructure without coarsening must be monitored. Mechanical grinding uses high-energy mixers, spherical balls, or tumbler mills. The refractor or balls deliver energy to the powder. The number of balls, rotation speed, size, ball/powder mass, grinding duration, and environment affect energy transmission. This synthesis method is ideal for making elemental, complex, and amorphous or nano-crystalline alloy particle powders [94].

1.2.2. Energy storage systems and supercapacitors

The reliance that modern civilization has on fossil fuels has resulted in a number of important problems, including escalating fuel costs, increased pollution, accelerated climate change, and heightened geopolitical conflicts [95]. In their efforts to lessen the impact of these problems on a global scale, governments have been placing a significant amount of emphasis on the development of alternative sources of energy and technology for energy storage. The location has been the impetus for a variety of study into the possibility of renewable energy sources such as wind, sun, compost, biogas, hydrothermal, and hot [96] . In point of fact, the electrical energies that are gleaned from this research find extensive application in a variety of facets of our day-

to-day existence. These power sources may be discovered in nature, and they convert kinetic energy into electrical energy. However, the amount of power they produce varies from time to time. Therefore, it is essential not only to get energy but also to store it and have it prepared to use with the appropriate outputs when those outputs are necessary. Capacitors, which are forms of energy storage devices, have been employed here up to this point. In order to manufacture devices of this nature, an insulating material must first be positioned between two conducting surfaces. In this configuration, when a source voltage is applied between the capacitor's plates, an effort is made for current to flow through the insulator, but the insulator serves as a barrier to the passage of electrons and prevents this from happening. Because of a phenomenon known as resistance, it is possible for energy to be stored in a dielectric material in the form of an electrical field. Therefore, the plates are able to store energy since they are charged in a variety of ways while at the same time [97]. The amount of capacitance it has depends on the dielectric constant of the material that is sandwiched between the plates. These results indicate that a high capacitance may be achieved by placing components with a high dielectric constant between two metal plates. It has been observed that perovskite-structured components with a high dielectric constant, including BaTiO_3 and SrTiO_3 , provide very high capacitance in this context [98]. As a result of their high capacitance value, polymers including polyaniline, PVDF, and metal oxides are used in a wide variety of electronic devices. However, modern technological advancements call for not just higher power output, but also higher energy density and a quicker charge-discharge cycle time [99]. Helmholtz hypothesized that a bigger energy storage capacity might be achieved without using materials with a high dielectric constant by decreasing the thickness of the dielectric material between the plates and increasing the surface area [100]. This is because double layer super capacitors as shown in Figure 1.5. have been developed [101]. These include a liquid electrolyte for ion exchange, a separator that allows ions to flow, and a conductor with a large dielectric surface area. The positively and negatively charged ions in the electrolyte migrate to the electrodes when the supercapacitor charges. Additionally, the thickness of the dielectric material at the contact is proportional to the size of the ions in the electrolyte (1nm). This thickness is often reduced to between 2 and 5 m in conventional capacitors. Capacitance has increased

by a factor of over a thousand when just thickness is taken into account. Therefore, supercapacitors are able to store more energy than conventional capacitors [102].

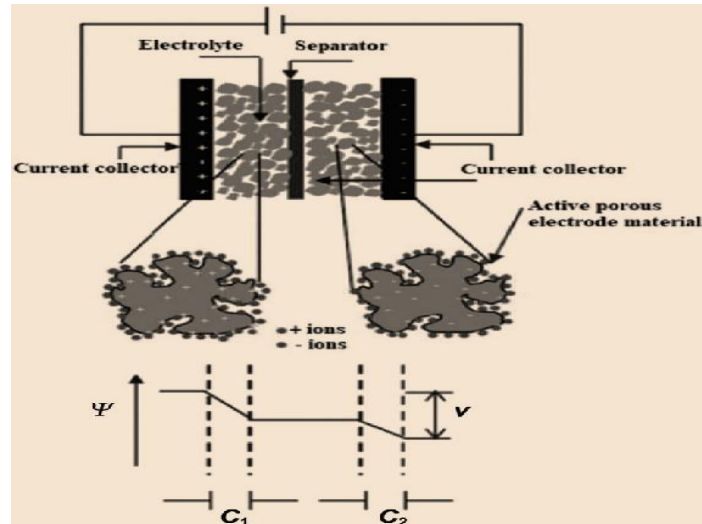


Figure 1.5. Schematic of porous electrode materials used in a supercapacitor [103].

1.2.3. Characterization of supercapacitor electrodes

Supercapacitors, a high energy storage device with unique properties, are well suited for a variety of applications due to their high-power density and robust electrochemical performance. Their industry has rapidly grown as a consequence. Supercapacitors may have uses in transportation, hybrid and electric vehicles, rail systems, memory backups, as well as other areas [104]. Supercapacitors are electrochemical capacitors made up of two porous electrodes with a large surface area that are immersed in an ionic electrolyte and separated by a porous structure that inhibits electrical short-circuiting while allowing ion flow [105]. Unlike batteries and fuel cells, which harvest energy stored in chemical bonds via faradic reactions at the anode and cathode, it is widely accepted that the properties of supercapacitors are primarily the result of three different charge storage mechanisms that can coexist and contribute in varying proportions in the same device [106]. Another process is based on the nanometer-sized electrostatic charge separation at the interface among both large surface area porous electrode material and the electrolyte (electric double layer), a mechanism has been contributed to high adsorption surface redox reaction through which partial faradic charge transfer that takes place between the pseudocapacitive electrode material and

the electrolyte, and a third one is due to diffusion-controlled ions intercalation. Each of these mechanisms contributes to the formation of the electric double layer. In general, a voltage-independent current in response to a linear voltage scan and a linear voltage-time profile in response to a constant-current charge/discharge of a supercapacitor are both indicators that the device in question is an electrical double-layer capacitor rather than a supercapacitor [107]. When particularly in comparison to rechargeable batteries, supercapacitors exhibit exceptional power performance (as high as 10 kW kg⁻¹), a greater degree of reversibility, and long cyclic life (>10⁶), all while remaining low-cost, repairs, and ecofriendly devices that can be easily integrated into electronic circuits and power systems. Supercapacitors also have a higher degree of reversibility than rechargeable batteries [108]. Thus, supercapacitors are extensively employed as energy storage devices in high-power applications such solar energy harvesting systems for autonomous field devices [109], renewable power systems [110], hybrid energy storage systems [111], electric cars [112] and biomedical implants [113]. Because of this, and because the different ways that charge is stored can lead to nonlinear behavior, it is important to know how well supercapacitors perform in any given application so that other parts of the system can be designed for the right current rating and life time [114]. The performance of supercapacitor devices is often evaluated using three metrics: capacitance, equivalent series resistance, and operating voltage. With this information, the amount of power and energy that is stored may be calculated [115]. The evident difference in both the time and frequency domain electrical characteristics of supercapacitors compared to excellent capacitors shows that present commercial standards and characterization methodologies for these devices need to be updated. Thus, supercapacitor's performance measurements will be exact, enabling their optimal use and applications. There are several research and review publications on supercapacitor characterization techniques [116], most assume that ideal capacitor relations can be directly applied to non-ideal supercapacitors. Additionally, it is troubling to note that the analysis often uses an ideal capacitors approach in the time domain despite the fact that the ac impedance data of these devices is frequently modeled with constant phase elements (CPE), which indicate the existence of dispersive behavior resulting from distributed relaxation time constants [117].

PART 2

LITERATURE REVIEW

2.1. SUMMARY OF PREVIOUS STUDIES

2.2.1. MnO₂ based supercapacitor electrodes

Xiuchang Chen et al prepared the MnO₂/MXene/cc (MTC) composite electrode by using a simple two-step electrodeposition method. Though, they realized that the MnO₂ compartment is affecting the charge/discharge process. They also observed that at a high density the performance increase. Therefore, their asymmetric flexible supercapacitor (MTC) (TC) showed a large voltage, a high energy density at a high-power density. So, a stable cycle (88% after 10.000) cycles[118] .

Dong et al. used the morphology of MnO₂ nanostructures to carry out the synthesis of a MnO₂-graphene foam hybrid with a regulated MnO₂ particle shape for use as a supercapacitor electrode, and they were able to readily adjust the acidity of the solution. They also show that this study proves the excellent potential of graphene foam to be utilized as new three-dimensional hybrid, giving a notable electrochemical properties (560 F/g at the current density of 0.2 A/g) and excellent cycling stability [119].

Zeenat et al. examined the simple synthesis of Bi₂O₃-MnO₂ nanocomposite material to create the electrode materials Bi₂O₃, MnO₂, and Bi₂O₃-MnO₂ on a graphite rod, an autocatalytic chemical technique called simultaneous ion layer adsorption and reaction (SILAR) is used to absorb electrolyte ions easily and quickly for improved energy storage efficiency. The X-Ray was used to explore how the composite matrix of Bi₂O₃ α-MnO₂ was formed. They discovered that the behavior of the battery and supercapacitor of Bi₂O₃MnO₂/Bi₂O₃ α-MnO₂, also is dominant to that of individuals

as well as those reported in previous studies for symmetrical electrochemical storage devices focused on Bi_2O_3 , MnO_2 , and Bi_2O_3 α - MnO_2 . The as-prepared compound electrode material confers 350 F g^{-1} specific capacity (SC) @ 10 A g^{-1} , which is better than that of an individual equivalents [120].

Kumara and Bhatia. Developed a large-area 3D structure of H- MnO_2 (NB) nanobricks by controlling the way Mn is deposited on a Cu substrate and then steam the structure at high temperatures in a hydrogen atmosphere. The electrochemical has a high specific capacitance of 1410 F/g and a high surface capacitance of 295 mF/cm^2 . It also has an elevated cycle stability (just 5% of the actual specific capacity is lost after 3000 cycles at a current density of 2.5 A/g). H- MnO_2 NBs work well as a supercapacitor electrode because the active material has better electronic and ionic conductivity. This is because there are hydroxyl groups on the layer of MnO_2 NBs [121].

Jiao et al. produced a 3D MnO_2 -ITO NWs composite having high specific surface area and low resistance as just an electrode material for SCs. Using tin-doped indium oxide nanowires (ITO NWs) composite with highly ordered network architectures for electrochemical supercapacitors to synthesis MnO_2 . The optimized MnO_2 has a high specific capacitance of 508.54 F g^{-1} at the scan rate of 5 mV s^{-1} , while the bare ITO NWs have a specific capacitance of just 2.83 F g^{-1} , making it possible to disregard the impact of the matrix material to capacitance. offers the chance to turn highly conductive materials into extremely effective pseudocapacitive SCs that may be utilized in various electronic items [122].

Zhao et al. Made using thiourea as a cross-linking agent, nitrogen source, and sulfur source. The precursor SA-based composite gel was Hierarchical N, S-co-doped porous carbon/ MnO_2 composites with an SSA of $1701 \text{ m}^2 \text{ g}^{-1}$ were generated by single-process carbonization. Besides that, adding KMnO_4 to porous carbon compounded MnO_2 and enhanced its pore structure. The pseudocapacitance created by MnO_2 's redox reaction gave NSPC/ MnO_2 a high specific capacitance of 281.1 F g^{-1} at 1 A g^{-1} as a SC electrode material. 86.02 % of original capacitance was retained after 5000 cycles at 10 A g^{-1} . A capacitance with a high specific value needed enough MnO_2

loading and a suitable pore structure. Porous carbons may be made easily and cheaply. It has incredible potential in SCs hybrid electrodes [123].

Kiymaz et al. In their research described the improved performance of nanostructured MnO₂ electrodes from a diffusion perspective. First, they described the morphological characteristics of flower-shaped MnO₂ nanosheet and MnO₂ nanowire with similar crystal structure (-MnO₂ phase) and capacitance-voltage characteristics. After that, using electrochemical impedance spectroscopy and a three-electrode configuration, the variables that limited the effectiveness of the bias voltage-dependent capacitance were described. Ion diffusion and charge transfer processes could be better understood through the information provided by resistance and capacitance frequency plots respectively [124].

Jiang et al. They carried out deposition of MnO₂ nanoparticles on the surface of the DMC support was examined utilizing multiple structural studies, including FT-IR, nitrogen adsorbent, XRD, XPS, SEM and TEM. Compared with DMC and MnO₂ electrodes, the DMC/MnO₂ nanocomposite demonstrated the greatest capacitive performance reaching 292 Fg⁻¹ at a current density of 0.5 Ag⁻¹. Additionally, DMC/MnO₂ has high cycle stability (21% capacity loss after 2000 charge cycles/dump) and throughput performance (61% capacity retention across 0.5 to 10 A g⁻¹). Additionally, with a particular power of 100 W kg⁻¹, a symmetrical two-electrode supercapacitor device offered a high specific energy of 34 W h kg⁻¹. The work done there will help with the development of high-performance supercapacitor technology [125].

2.2.2. Ti₃C₂T_x based supercapacitor electrodes

Binxia Chen et al aimed to improve the supercapacitor's electrode capacitance. Therefore, they integrated positively charged PANINIS into MXene (Ti₃C₂T_x) Nano sheets. Therefore, the change of the morphology and the porous structure of the composite explain The MP composite electrode's high competence. They also said that the electrode has stabilized during the charge/discharge process. So, the cycle stabilized as well [126].

Wu et al. Explored the negatively charged electrode in supercapacitors, free-standing $\text{Ti}_3\text{C}_2\text{T}_x$ sheets are made by etching Ti_3AlC_2 powders in a solution of HCl and LiF, followed by vacuum filtering. After testing the electrochemical performance of $\text{Ti}_3\text{C}_2\text{T}_x$ paper, a high volumetric capacity of 295.4 F cm^{-3} was discovered. Furthermore, it had a high-capacity rate of 79.7% from 2 mV s^{-1} to 100 mV s^{-1} , as well as a long useful life with an initial sound stability of 94.4% after 15 000 charging and discharging cycles at a current density of 10 A g^{-1} . The UPS unit has a power density of 1.3 kW kg^{-1} and an energy density of 4.5 Wh kg^{-1} . The device's application has been shown by lighting a red light-emitting diode, allowing the use of $\text{Ti}_3\text{C}_2\text{T}_x$ -paper as the negative electrode in supercapacitors [127].

Zhang et al. have synthesized a flexible electrode from multi-scaled $\text{Ti}_3\text{C}_2\text{T}_x$ by vacuum filtering of HF-etched nanoparticles and HCl + LiF-etched nanosheets. The $\text{Ti}_3\text{C}_2\text{T}_x$ -10 flexible has a greater specific capacitance of 372 F g^{-1} at 1 A g^{-1} than the film, and it retains 95% of its capacitance after 5000 cycles. Even while the generated flexible electrode based on multi-scaled MXene has a larger specific capacitance than previously reported MXene composites and graphene composites, it is still marginally less capacitance than surface modified MXene films and N-doped MXene electrodes [128].

Whang et al. came up with a plan to make 3D aerogel with 1D channels using directed freeze drying of $\text{Ti}_3\text{C}_2\text{T}_x$. The 3D $\text{Ti}_3\text{C}_2\text{T}_x$ /Sodium alginate (SA) aerogel is able to efficiently handle the stacking issue of $\text{Ti}_3\text{C}_2\text{T}_x$ nanosheets with the assistance of the unidirectional channels, and it also speeds up the diffusion of ions. The $\text{Ti}_3\text{C}_2\text{T}_x$ /SA-5 electrode may still attain the mass capacitance of 284.5 F g^{-1} and the areal capacitance of $4030.4 \text{ mF cm}^{-2}$ at 2 mV s^{-1} when the loading is 14.2 mg cm^{-2} in $1 \text{ M H}_2\text{SO}_4$ electrolyte. Both of these capacitances are measured when the electrode is subjected to a voltage of 2 mV s^{-1} . In addition, the electrode demonstrated excellent cycling performance after 20,000 cycles at 50 mV s^{-1} , with no deterioration of the capacitor occurring during this time. These findings imply that high performance supercapacitor electrodes with high mass loading may be manufactured by using the method of

creating a specific three-dimensional structure of two-dimensional MXene with one-dimensional channels that run in only one direction [129].

Javed et al. suggested increasing energy density by using a heterostructured (HS) composite of nickel-cobalt-sulfide (NCS) nanoflowers embedded in exfoliated $Ti_3C_2T_x$ MXene layers (HSNCS@MXene). The NCS nanoflowers created a sandwich-like structure inside the MXene layers. Using a three-electrode setup, the HSNCS@MXene showed very impressive pseudocapacitive performance. They measured a capacitance of $2637 F g^{-1}$ ($1582 C g^{-1}$) at $2.5 A g^{-1}$ and found that it was stable across 10,000 cycles, maintaining 96% of its starting value beyond that point. The charge storage method in HS–NCS@MXene composite involves Faradic and electrochemical double-layer storage, according to postmortem analyses. HS–NCS@MXene with activated carbon formed an AHSC (HS–NCS@MXene/AC–AHSC). The HS–NCS@MXene/AC–AHSC operates in a potential range up to 1.6 V and delivers a high capacitance of $226 F g^{-1}$ at $1.5 A g^{-1}$ with steady cyclic life (92%) up to 20,000 cycles. The HS–NCS@MXene/AC–AHSC has an energy density of $80 Wh kg^{-1}$ and a power density of $1196 W kg^{-1}$, surpassing most previous publications. AHSCs' electrochemical performance is enhanced by the HS–NCS@MXene composite's synergy [130].

2.2. THE OBJECTIVE OF THIS STUDY

In order for this thesis to be carried out successfully It is aimed to synthesize carbon fabrics as flexible electrode material and $Ti_3C_2T_x$ structure to be used as additive material, synthesize nanotube geometry MnO_2 crystals together in different ratios between $Ti_3C_2T_x$ layers and on carbon fabric surfaces also characterize whether the produced electrodes consist of the desired components in the targeted size and geometry with the BET analysis of each electrode to determine the surface area and pore size changes.

It is aimed to carry out SEM and TEM analyzes to check whether the synthesized components on the electrode surfaces are in the desired geometry and location characterize whether the synthesized components on the electrode surfaces are composed of targeted MnO_2 and $Ti_3C_2T_x$ components by XRD, XPS, FTIR and Raman

analyzes. Secondly, it is meant to analyze the electrochemical tests of the produced electrodes and the chemical interactions of electrolyte liquids. In order to characterize the electrochemical performance of the produced electrodes, also to perform cyclic voltammetry, charge-discharge and impedance measurements at different test parameters.

For the purpose of examine the chemical interactions of the produced electrodes with the electrolyte liquid, its purpose is to examine the crystallographic, microstructure and bond energies, respectively, by XRD, XPS and SEM analyzes of the electrode surfaces after the test. It is focused on determine the performance in real ambient conditions by converting the electrodes with the optimum performance obtained in the examinations in the first and second objectives into symmetrical supercapacitors. It is aimed to produce an asymmetrical supercapacitor with the electrode(s) with the most optimum performance. At this stage, it is directed towards use activated carbon impregnated carbon cloth as the counter electrode and a mixture of H₂O/PVA/Na₂SO₄ as the electrolyte. In order to determine the behavior of the produced supercapacitors under real ambient conditions, it is designed to measure their electrochemical performances at three different temperatures (<0°, 25° and 50°) and determine the behavior of the produced supercapacitors in real conditions, it is aimed to measure the electrochemical performances during the bending behavior at 90° and 180°.

PART 3

EXPERIMENTAL PROCEDURE

3.1. MATERIALS AND METHODS

3.1.1. Carbon fabric production

After making a mixture of ethanol, distilled water and acetone at a ratio of 1:1:1 in a beaker, a piece of cloth cut in 5x5 cm dimensions was dipped in this mixture for 10 minutes and then dried in an oven at 60 °C for 48 hours. Thus, it is ensured that organic residues on the fabric are removed. Then, the piece of fabric was taken to the atmosphere-controlled tube furnace as shown in Figure 3.1. And heated up to 800 °C in the presence of argon gas with a temperature increase of 5 °C per minute and kept at this temperature for 60 minutes. Then, when the temperature of the oven reached room condition, the cover was opened, and the carbonized fabric piece was taken. The electrical conductivity of each fabric obtained was checked with a multimeter. The resistivity of the carbonized fabric here was determined to be $3.5 \times 10^{-8} \Omega \cdot m$ in the measurement made with a multimeter. The fact that this value is very close to aluminum ($2.8 \times 10^{-8} \Omega \cdot m$) indicates the suitability of the produced carbon fabric to be used as a current collector. In addition, nickel foam with a resistivity of $6.99 \times 10^{-8} \Omega \cdot m$ is widely used in supercapacitors, and the carbon fabric obtained as a preliminary study can be said to be a current collector in terms of conductivity.

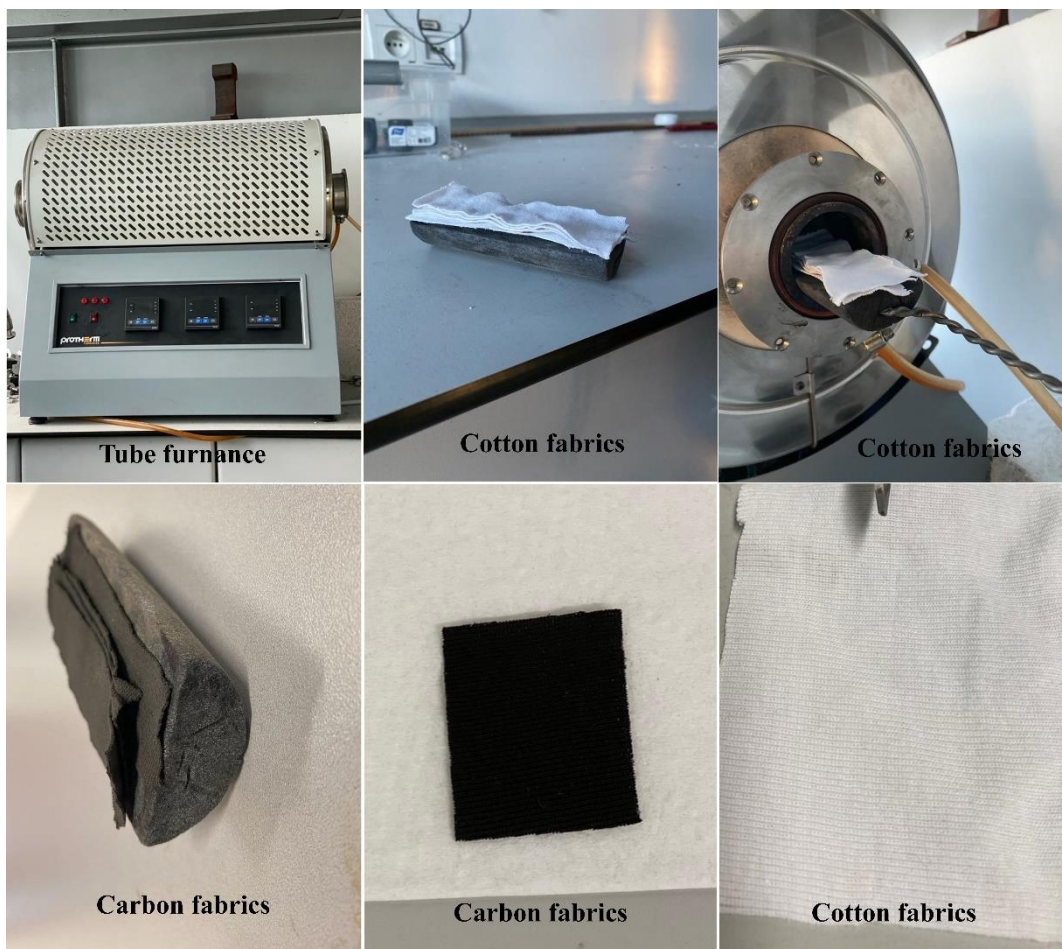


Figure 3.1. Chalcopyrite unit cell (Cu: red, Fe: blue and S: yellow color)

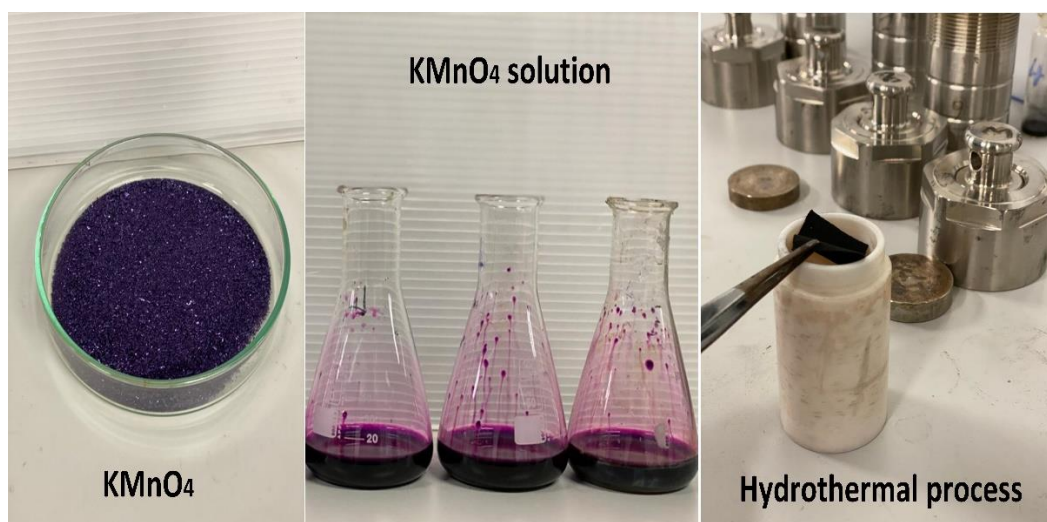


Figure 3.2. Production stages by hydrothermal method

3.1.2. $\text{Ti}_3\text{C}_2\text{T}_x$ synthesis

The MXene structure ($\text{Ti}_3\text{C}_2\text{T}_x$) is a layered void structure obtained by removing the A layer in the MAX phase. To obtain this structure, the method applied by Mahmood et al. was used [131]. First, 1 gram of Ti_3AlC_2 powder, which is the MAX phase, took and transferred to a polyethylene container with a lid and 20 ml of 40% concentration HF liquid added slowly. Then the container closed, and the etching process carried out by mixing with a magnetic stirrer at 200 rpm for 24 hours. After this process, the products centrifuged at 500 rpm for 5 minutes, washed with distilled water until the pH of the mixture becomes 7, and then dried in an oven at 80 °C for 10 hours. After these processes, the delamination of the MXene layers ensured by taking the appropriate amount for electrode production and mixing it ultrasonically in 20 ml of dimethyl sulfoxide for 50 minutes. Two magnetic stirrers used in this study.

3.1.3. $\text{MnO}_2@ \text{Ti}_3\text{C}_2\text{T}_x$ synthesis on CC surfaces

Xiao et al. carried out the hydrothermal synthesis of nanotube geometry MnO_2 crystals using 1:4 and 1:3 ratios of $\text{KMnO}_4\text{-HCl}$ at 140 °C for 12 hours and obtained the pore sizes as 180 nm and 80 nm, respectively [132]. According to the results obtained, it is seen as a deficiency that this method is applicable in terms of production, but that the $\text{KMnO}_4\text{-HCl}$ ratio (especially the amount of HCl) is not evaluated in a wide enough range. In addition, it has been observed that the amount of secondary component such as $\text{Ti}_3\text{C}_2\text{T}_x$ to be added to the solution has been tried as only 5 mg in the literature [133]. The change in the amount of secondary components in such productions can affect the geometry of crystals such as MnO_2 that form in the environment. In this thesis, these deficiencies could be solved by changing them in terms of $\text{KMnO}_4\text{-HCl}$ ratio and $\text{Ti}_3\text{C}_2\text{T}_x$ amount as in Table 3.1. For this purpose, firstly, 80 Mg KMnO_4 and 20 μl hydrochloric acid dissolved in 10mL deionized water by magnetic stirring. Then, 5 mg of $\text{Ti}_3\text{C}_2\text{T}_x$ added to this solution and mixed in an ultrasonic mixer for 2 hours. In the meantime, 1x2 cm^2 size cut from the previously prepared carbon fabric, the surfaces washed with deionized water. After these processes, the final mixture and carbon fabric transferred to a 40mL Teflon lined stainless steel autoclave as seen in Figure 3.3. And the synthesis process carried out by heating in a muffle furnace at

130°C for 10 hours. Then, the autoclave removed from the oven and cooled to room temperature, and the carbon fabric inside removed and washed with distilled water to remove any residues that may exist on it. After this process, it placed on a watch glass and transferred to the oven again and kept at 60°C for 24 hours. This process carried out to remove moisture and ripen the crystals. Thus, the production process of the M2 electrode completed. All other electrodes similarly fabricated by only making the concentration changes in Table 3.1.

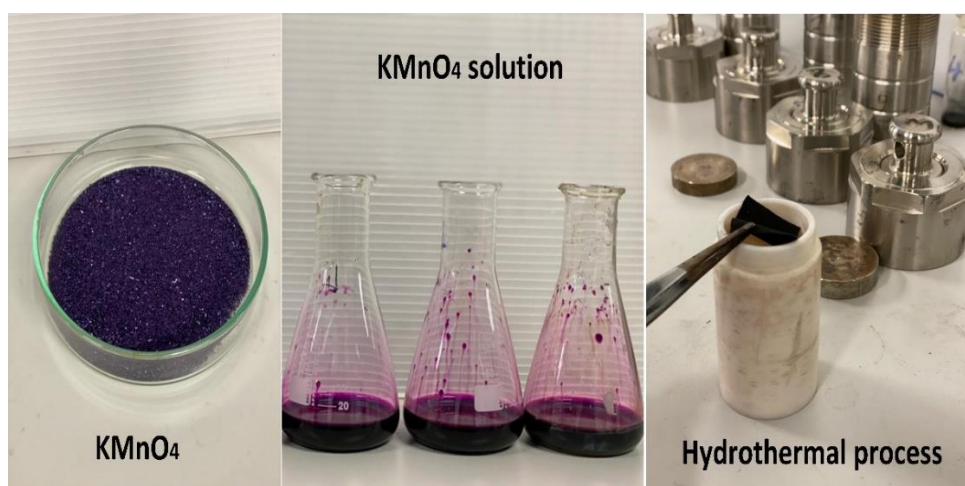


Figure 3.3. Production stages by hydrothermal method

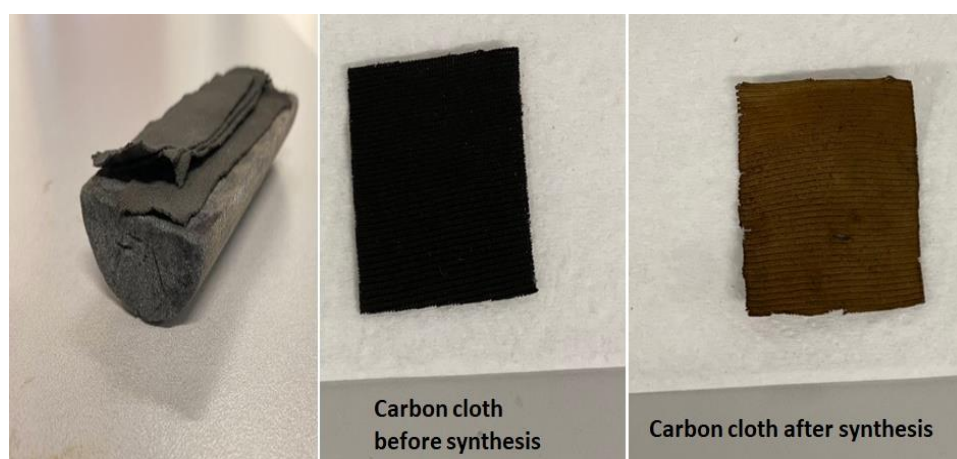


Figure 3.4. Digital image of carbon fabrics before and after synthesis

Table 3.1. Production parameters.

	KMnO₄	MXene	HCl	DW
M1	80 mg	0	20 μl	10 ml
M2	80 mg	5 mg	20 μl	10 ml
M3	80 mg	15 mg	20 μl	10 ml

3.1. MATERIAL CHARACTERIZATION

The production of electrode materials examined in terms of quality and quantity. Firstly, all the electrodes produced for preliminary detection analyzed by X-ray diffraction pattern (XRD) and Fourier transform infrared spectroscopy (FTIR) and the presence of MnO₂@Ti₃C₂T_x additives on carbon fabric surfaces examined in terms of crystallographic and chemical bonding, respectively. According to the results obtained from here, surface area-pore size graphs drawn depending on the concentration and 3 electrodes with the largest surface area-pore size selected for each letter parameter in Table 3.1. Thus, one electrode with the largest surface area-pore size determined from each of the M1-M2-M3 production parameters. With this process, both the effect of KMnO₄-HCl ratio on the surface area-pore size of MnO₂ and the effect of Ti₃C₂T_x in quantity compared. On the other hand, by examining these 3 electrodes in terms of microstructure and morphology with scanning electron microscope (SEM) and transmission electron microscope (TEM), it observed whether MnO₂ nanotubes could synthesized in the desired geometry and size on the carbon fabric surface and between Ti₃C₂T_x layers. Figure 4.1. Shows the instruments used in this process. In addition, interplanetary distances (d-space) in structures synthesized by high resolution transmission electron microscopy (HRTEM) examined. It is aimed to confirm that the d-space values to be determined by HRTEM analysis belong to the planes of MnO₂ and Ti₃C₂T_x observed in XRD analysis. On the other hand, the binding energies of Mn, O, Ti, C and Tx (F or Cl) elements determined by examining the electronic configurations of the 1s and 2p orbitals by X-ray photoelectron spectroscopy (XPS) of the components of these 3 samples. According to the results obtained from here, MnO₂ and Ti₃C₂T_x formations confirmed.



Figure 4.1. Representation of instruments.

3.2. ELECTROCHEMICAL CHARACTERIZATION

The electrochemical performances of the produced electrodes measured using the PARSTAT 4000 potentiometer and a three-electrode cell system in the MARGEM laboratories of Karabuk University. In these measurements, Ag/AgCl used as the reference electrode, graphite rod as the counter electrode, and electrodes that have undergone production and characterization processes as the working electrode as illustrated in Figure 4.4. For the measurements, a 1 M concentration of Na₂SO₄ solution prepared with deionized water filled into a 100 ml electrolyte cell. Then, the reference, counter and working electrodes placed in the cell and the cables connected. 3 electrodes selected from the electrodes produced in the parameters Table 3.1. Used as the working electrode. Since the electrodes contain nano-sized pores, they kept in the electrolyte for at least 15 minutes so that they are completely wet before starting the measurements. Then, firstly, cyclic voltammetry and then charge-discharge measurements performed for electrochemical characterizations. Cyclic voltammetry (CV) measurements performed at a scanning rate of 10 mV/s in the potential range of 0-0.9V. This range was chosen in accordance with the electrode potential of MnO₂ specified in the literature [134]. After the CV measurements of the mentioned 3 electrodes, the specific capacitance values of each electrode calculated according to the formula in equation 3.1 [135].

$$Cs = \frac{I \times \Delta t}{\Delta V \times S} \quad (3.1)$$

In this formula $\int_{v_1}^{v_2} idv$, the area in the middle of the current voltage graph, m the mass of active substance on the electrode surface, v it represents the scanning speed and $(v_2 - v_1)$ represents the potential range at which scanning is performed. For the electrode with the highest capacitance observed here, cyclic voltammetry measurements performed again, but the scanning rates repeated by increasing 10 mV/s from 10 mV/s to 200 mV/s. The reason why the measurements are carried out at different scanning rates (I) to understand whether the reactions occurring at the electrode-solution interface are reversible and (II) to understand whether the redox process is diffusion or adsorption controlled [136]. Thus, by determining the behavior and specific capacitance values of all electrodes at a scanning speed of 10 mV/s, a comparison made in terms of component-geometry-size. After these measurements, galvanostatic charge-discharge (GCD) measurements planned to determine the charge-discharge times of the mentioned electrodes and to determine their electrocatalytic activities. First, as in the study of Zhang et al., the GCD measurement of these electrodes made at 1 A/g current density [136] and the C_{sp} value calculated according to the formula in equation 3.2 [107].

$$C_{sp} = \frac{I \times \Delta t}{m \times \Delta V} \quad (3.2)$$

In this formula, I represent the discharge current (A), the discharge time, the measuring potential range, and m the amount of active substance on the electrode surface. According to the result obtained from here, the electrode with the highest specific capacitance determined and the charge-discharge times of this electrode at current densities of 2, 4, 6, 8, 10 A/g determined. In addition, 1000 charge-discharge measurements made on the electrode with the highest specific capacitance, and the decrease in the specific capacitance value revealed. Thus, the specific capacitance values of the 3 electrodes at constant current densities determined and the results compared according to both the surface area and pore size changes and the effect of Ti_3C_2Tx . On the other hand, the behavior of the highest performance electrode at different current densities and the charge-discharge lifetimes after multiple cycles also determined. In addition, the energy density (E_d) (Wh/kg) and power densities (P_d) (W/kg) of the specified electrodes calculated according to the formulas specified in

equations 3.3 and 3.4 below .The explanations of the parameters in these formulas are given in the previous formulas.

$$E = \frac{Cs \times V^2}{7.2} \quad (3.3)$$

$$P = \frac{3600 \times E}{\Delta t} \quad (3.4)$$

In addition, the 3 electrodes mentioned are 100 kHz and 0.1 Hz. By performing impedance measurements in the frequency range, equivalent series resistances against currents at different frequencies determined .Thus, interpreted whether the $Ti_3C_2T_x$ additive increases the conductivity of MnO_2 . After these processes, electrochemical measurements completed. After all these measurements, one electrode with the best performance determined from the electrodes produced in the parameters in Table 3.1. Apart from these, the dimensional changes of the particles on the electrode surfaces, crystallographic and chemical bond changes examined by SEM, XRD and XPS analyzes, respectively, after 1000 cycles of measurements made to determine the cycle life of the electrode with the highest performance.

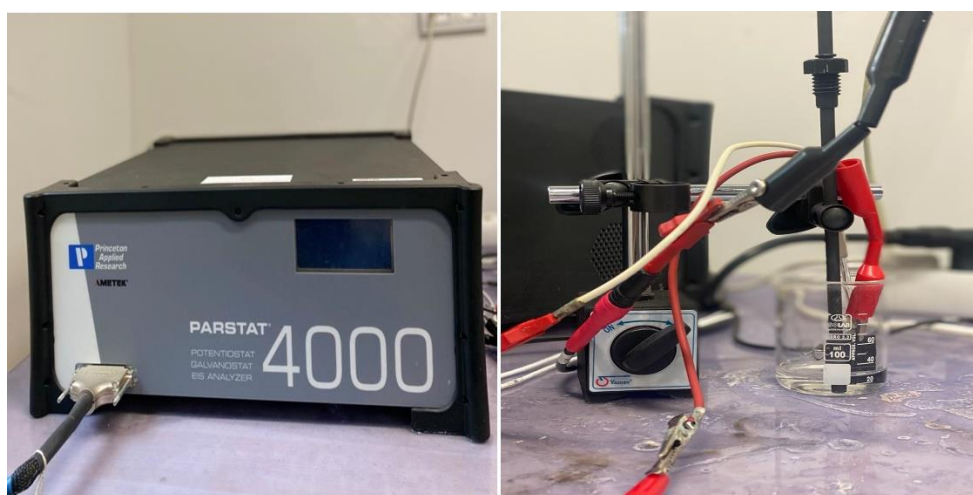


Figure 4.4. Three-electrode electrochemical measuring system.

PART 4

EXPERIMENTAL RESULTS AND DISCUSSION

4.1. MATERIALS CHARACTERIZATION RESULTS

In the first work package in this thesis, it is aimed to convert cotton fabrics into conductive carbon fabrics at high temperature in an oxygen-free environment and to convert the MAX phase to MXene. The obtained carbon fabrics are given in the characterization stage. Its conductivity was checked with a multimeter, and it was concluded that it was qualitatively conductive. On the other hand, the conversion process from MAX phase to MXene is aimed to be characterized by XRD analysis. The results are given in figure 4.1. According to these results, the 2θ value of $Ti_3Al_2C_3$ constituting the MAX phase is approximately 10° , 20° , 35° , 39° , 41° , 48° and 56° (002), (004), (101), (104), respectively. Peaks belonging to the, (105), (107), and (109) planes were observed. The transformation of the MAX phase into MXene is the solution of the aluminum in it, and the most important sign of this is the shift of the peak at 10° to the left. This shift ranged from about 9.5° to 7.2° . For this reason, it can be said that the production was successful.

In the second stage, MnO_2 synthesis is done by hydrothermal method on carbon fabric surfaces. This synthesis was carried out with MXene contributions. The obtained results were given in figure 4.2. Sample codes M1, M2, and M3 here were given in Table 3.1. Accordingly, the 2θ value belongs to the (110), (101), (211), (220), (002) and (310) planes at approximately 25° , 37° , 55° , 64° , 66° and 70° , respectively peaks were observed. In studies in the literature, it has been said that these peaks originate from the beta phase of MnO_2 crystals. However, it was observed that extra peaks occurred in some regions. These were also found to be related to the alpha phase of MnO_2 . As a result, it was understood that our synthesis was successful. On the other

hand, no extra peaks for MXene were observed in these synthesized constructs. This is due to the dense and intense MnO_2 crystals.

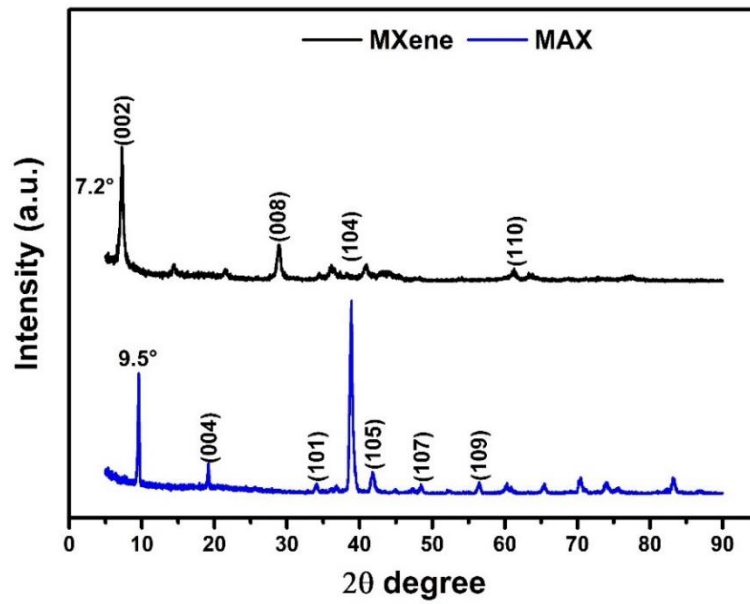


Figure 4.1. XRD analysis of MAX phase to MXene conversion

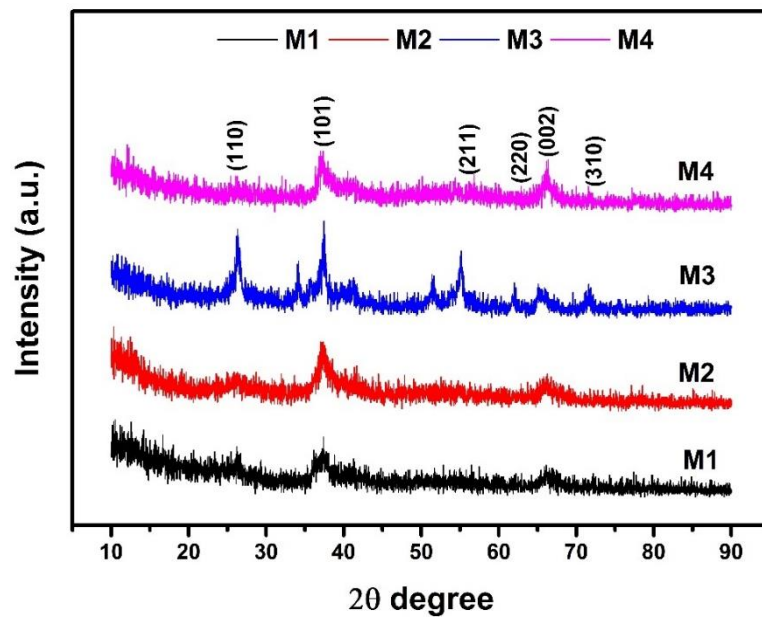


Figure 4.2. XRD analysis results of products after MnO_2 synthesis

Microstructure and morphology of these synthesized structures were investigated by scanning electron microscope (SEM) and transmission electron microscope (TEM). The results are detailed in figure 4.3. In the first two of these images (figures 4.3a and b), the surfaces of pure carbon fabric are given. In these images, it is seen that carbon fabrics are approximately 5-10 microns thick, smooth but curved. In Figure 4.3c and d, M4 and M1 samples are given as a representative. In the image of M1, it has been observed that crystal structures smaller than about 50 nm occur in needle-like form on the surfaces of carbon fabric fibers. The uniformity of these structures is very advantageous. Sample M4 has similar acicular structures, but extra lumpy and nodular structures are also seen. It is thought that these lumps are probably formed by the adhesion of MXene to the surfaces and the formation of MnO₂ crystals on it. However, MXene structures could not be clearly observed in these SEM images. For this, TEM analyzes given in figures 4.3e and f were carried out. In these images, it is seen that the bars are longer than 100 nm but smaller than 50 nm. On the other hand, it can be said that the dimensions are approximate and vary. In addition, the rectangular plate-shaped layered structures marked with arrows in Figure 4.3f are thought to be MXene. The observation of similar structures in the literature confirms these results. As a result, it can be said that MXene doped acicular MnO₂ crystals were successfully synthesized on carbon fabric surfaces.

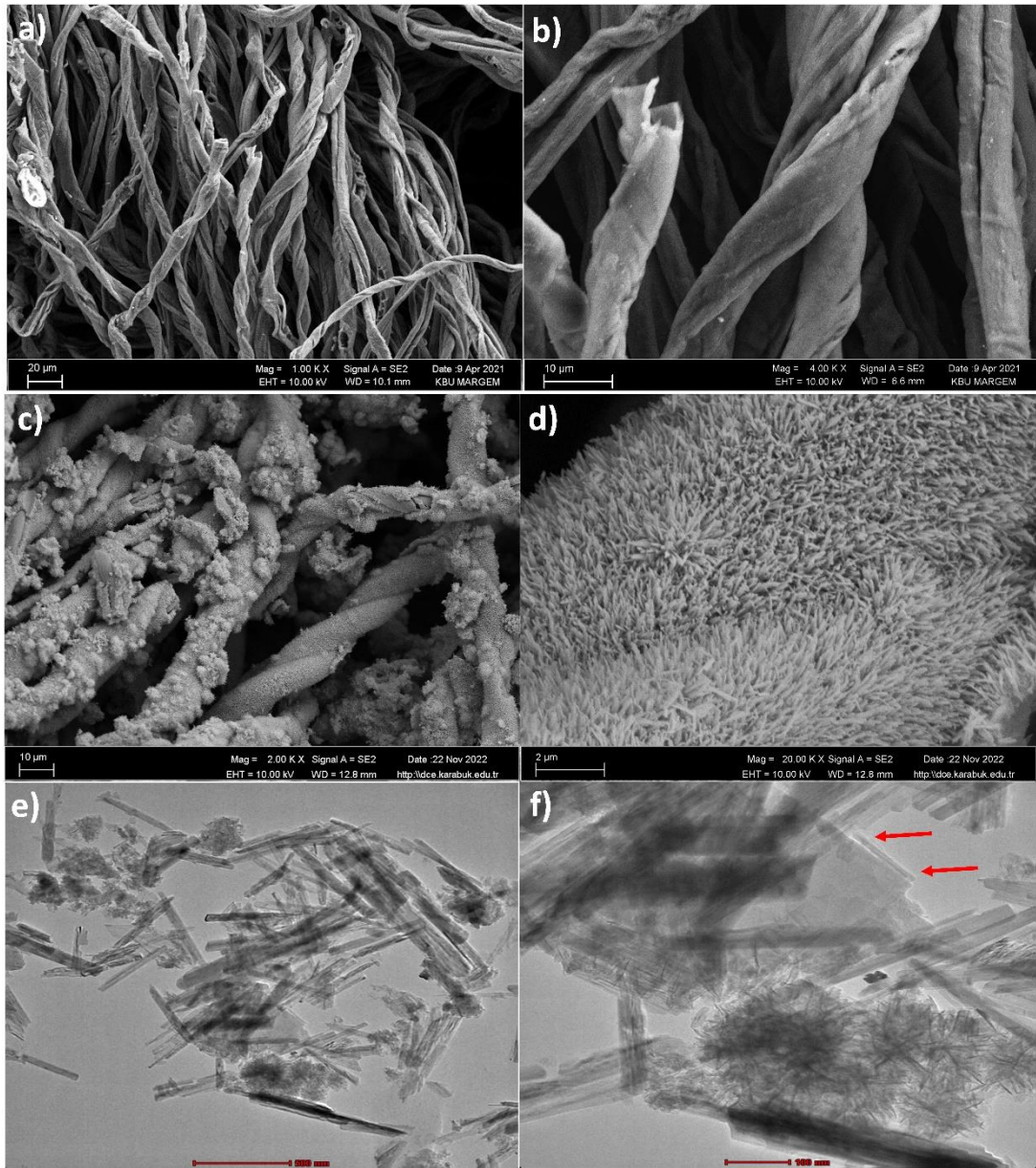


Figure 4.3. SEM images of a-b) carbon cloth, c-d) MnO₂ and MXene doped carbon cloth and e-f) TEM image of MXene and MnO₂ doped carbon fabrics.

4.2. ELECTROCHEMICAL MEASUREMENT RESULTS

First, cyclic voltammetry (CV) measurements were performed to examine the electrochemical performance of the electrodes. Scanning rates of 0.01 mV/s, 0.031 mV/s and 0.07 mV/s were applied for each electrode. The results obtained are given in figure 4.4, figure 4.5 and figure 4.6. According to these results, it was observed that it gave peaks in the anodic and cathodic regions. It is understood that these peaks are around 0.5 V in the anodic region and around 0.3 V in the cathodic region. These peaks are thought to result from oxidation and reduction as well as from diffusion of ions to the electrode surface. Depending on the amount of diffusion of ions to the electrode surface or the amount of redox reactions, the peak intensities and integral area of each sample changed. In addition, it can be said that the electrodes have a battery type charge storage mechanism due to these peak

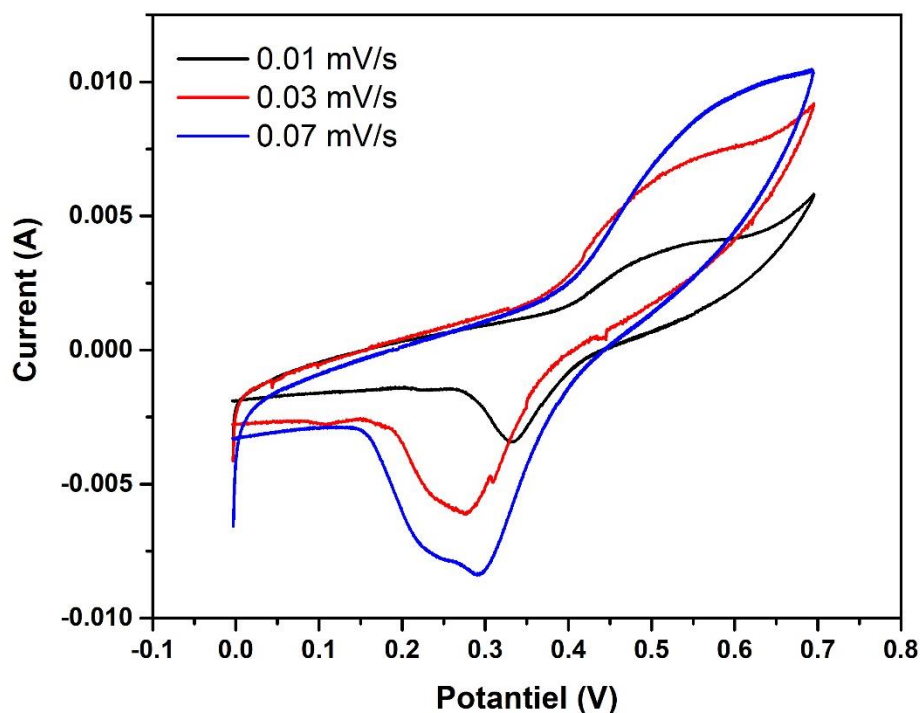


Figure 4.4. CV curves of M1 sample

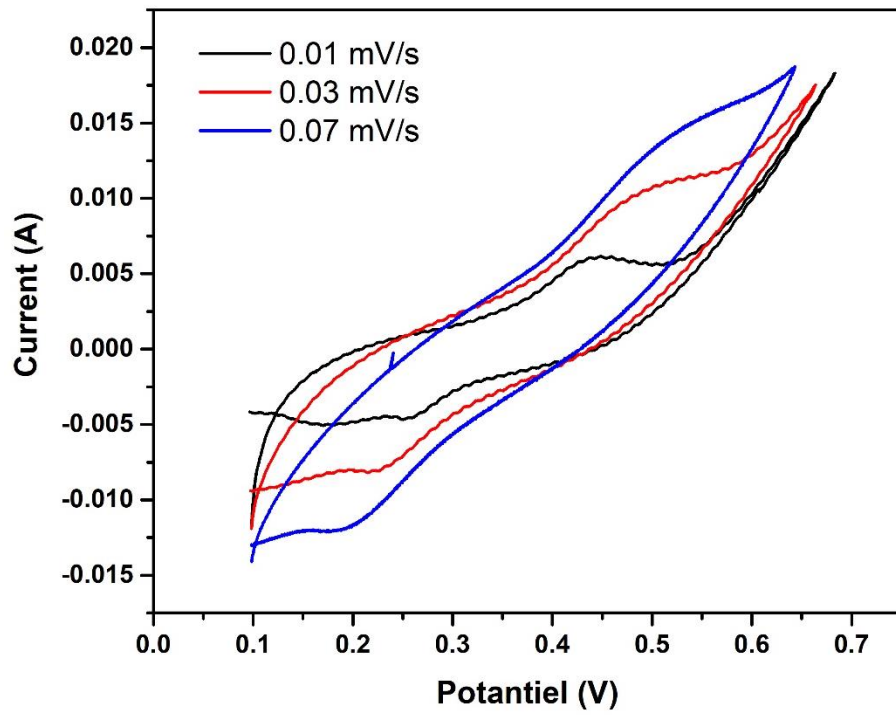


Figure 4.5. CV curves of M2 sample

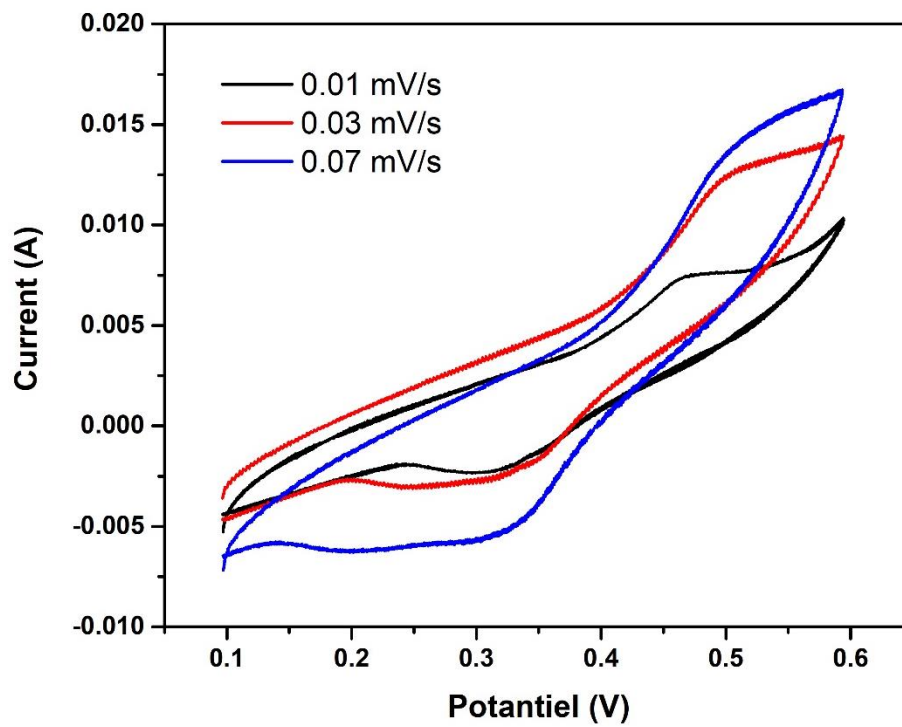


Figure 4.6. CV curves of M3 sample

In terms of electrochemical performance, charge-discharge measurements of these electrodes at different scanning rates were also performed. The current values applied in the measurements were changed from 1 mA to 7 mA. The results obtained in figure 4.7, figure 4.8 and figure 4.9 are given. According to these results, the discharge times of the MXene undoped electrode (M1) at 1, 2, 3, 4, 5, 6 and 7 mA were determined as 189s, 91s, 57s, 31s, 28s, 23s, and 19s, respectively. Similarly, the discharge times of the 5 mg MXene added M2 sample were measured as 296s, 140s, 76s, 48s, 32s, and 25s, respectively. When the amount of MXene is increased to 15 mg, it has been calculated that the discharge time reaches 1140s, 418s, 214s, 140s, 85s, 56s, and 38s, respectively. Two things emerge from this: (I) the discharge time decreases as the current increases and (II) the discharge time increases as the MXene amount increases. As the current increases, the prolongation of the discharge time is associated with the ions reaching the electrode surface [137,138]. It is known that at high currents, the ions in the solution quickly reach the electrode surface and form a film layer, so they cannot pass into the inner parts of the electrode. Following this, rapid return of the discharge shortens the discharge time. However, when low currents are applied, it is possible for the ions to reach the electrode surface slowly and hold on, and thus reach the inner orbits of the electrode [139,140]. On the other hand, the transition of ions to the solution takes place very slowly and the discharge time is considerably longer. The extension of the discharge time here actually means that the electrode can hold more ions, and the energy storage capacity is evaluated from here. Another important point is that as the amount of MXene increases, the discharge time is prolonged. The main purpose of this study was based on the hypothesis that this would happen anyway. According to this hypothesis, if a two-dimensional component was added to the electrode, the ion holding capacity would increase due to its large surface area and the energy storage capacity would increase. It can be said that an increase of only about 56% occurs when the MXene supplement is 5 mg, but this increase reaches its peak with the 15 mg supplement. It is thought that not only MXene but also MnO₂ nanorods synthesized together with MXene contributed significantly to this increase. Studies in the literature so far are in this direction. For this reason, it is thought that it is very important to bring the hypothesis to be realized and the changes in the results depending on the amount of MXene to the literature.

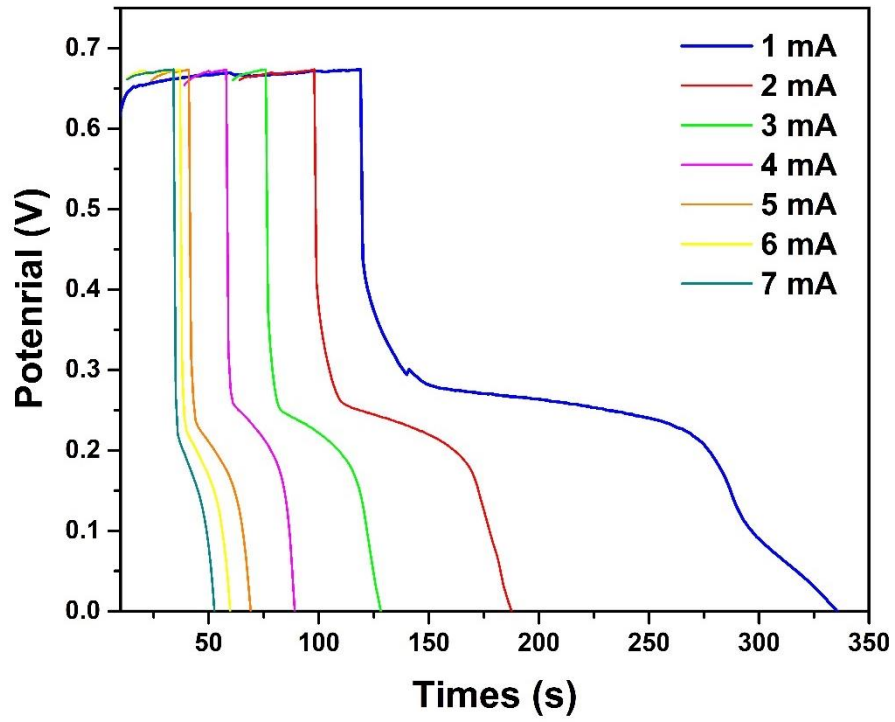


Figure 4.7. GCD curves of M2 sample

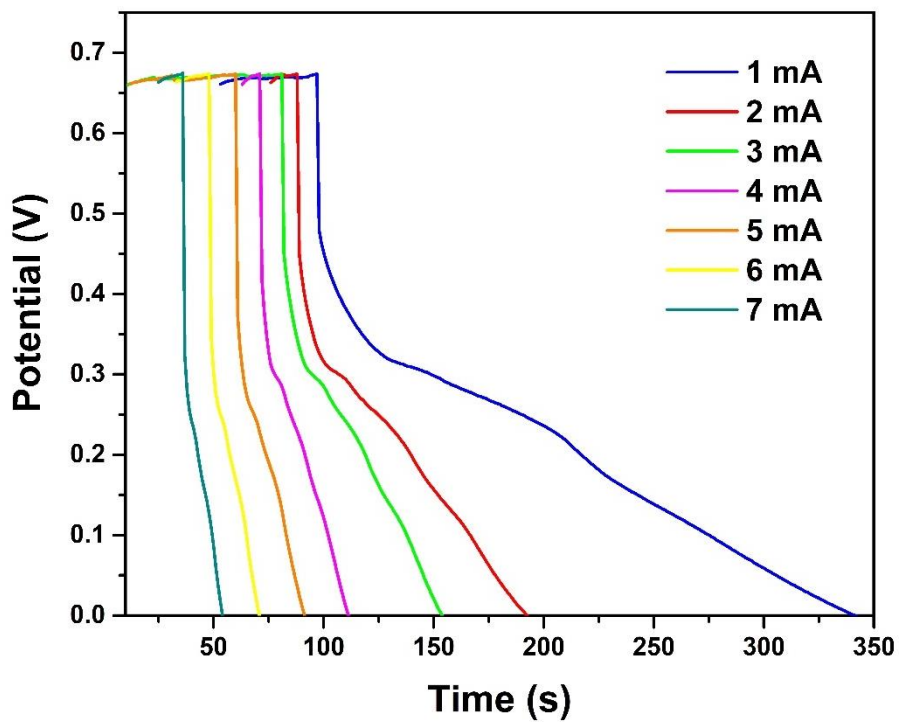


Figure 4.8. GCD curves of M2 sample

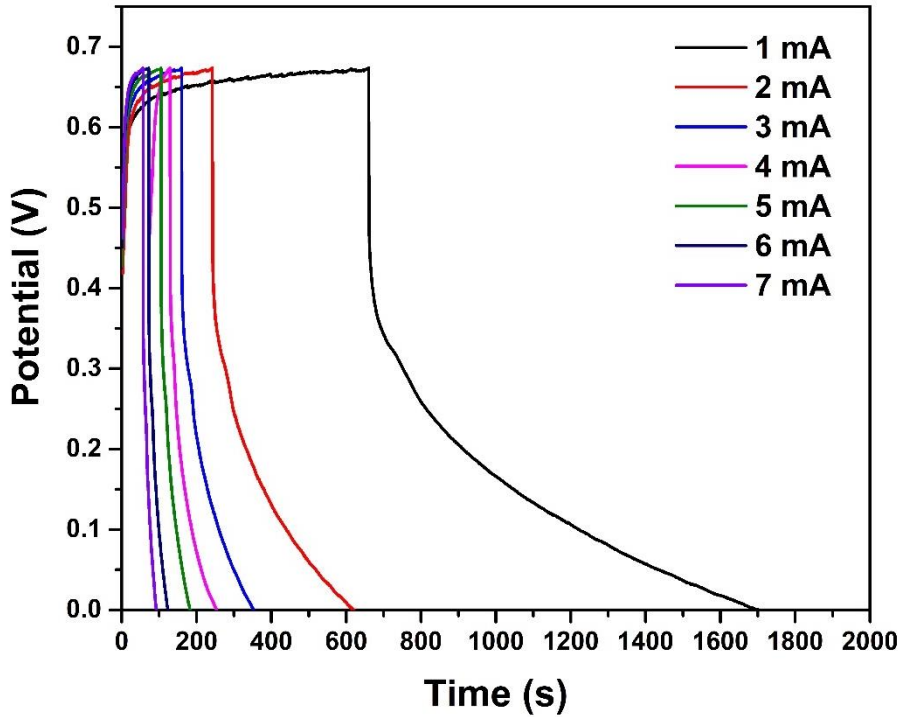


Figure 4.9. GCD curves of M3 sample

According to the equation 3.1 given in the characterization part of these electrodes, firstly, the specific capacitance values were calculated. The results are given in figure 4.10. According to these calculations, the specific capacitance of the M1 sample from 1 to 7 mA was found to be 182, 175, 165, 119, 135, 133 and 128 mF/cm^2 , respectively. The specific capacitance of the M2 sample was calculated as 285, 270, 220, 185, 154, 144 mF/cm^2 from 1 to 6 mA. According to these values, the MXene add-on increased the specific capacitance, probably due to the large two-dimensional surface area. However, the specific capacitance of the M3 sample was calculated to be approximately 1100, 807, 620, 541, 410, 324 and 257 mF/cm^2 . Although the amount of MXene increased almost three times, the specific capacitance values increased about 4 times. Here, it probably caused the formation of MnO_2 on a larger surface with the increase in the amount of MXene, which created such a synergistic increase.

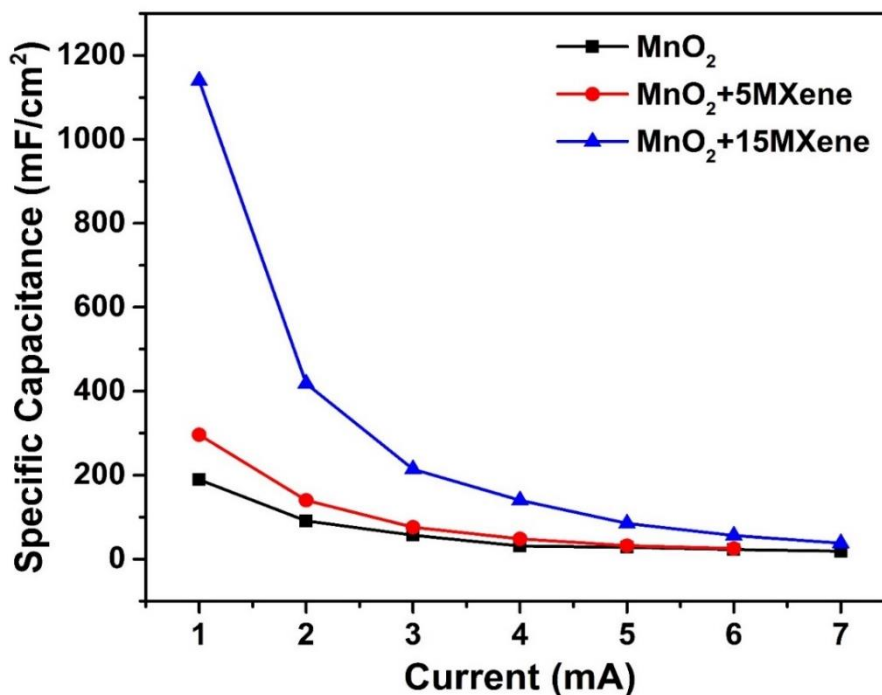


Figure 4.10. Specific capacitance values of electrodes

Apart from these, the energy (E) and power (P) densities of these electrodes at the aforementioned currents were also calculated. Calculations were made according to equations 3.2 and 3.3 in the electrochemical characterization part. The results are given in figure 4.11. According to these results, the highest energy and power density values of the MXene undoped M1 electrode were determined as 12 mWh/cm² and 230 mW/cm². Power density values did not change in other samples. However, the energy density values increased. According to the calculations, the E value of the M2 sample was found to be 18.9 mWh/cm², while the E value of the M3 sample was 72.8. As a result, a natural cotton fabric was first carbonized at high temperature in an oxygen-free environment. Thus, a structure that is both conductive and flexible has been created. This carbon fabric alone has very low specific capacitance and energy density values. Therefore, its surface needs to be functionalized. For this purpose, manganese oxide synthesis was carried out by hydrothermal method on its surface. The formation of MnO₂ crystals on fabric surfaces in the form of needle-like nanorods both widened the surface of the fabric and made it functional for redox reaction with ions. The results obtained here are in line with the literature. However, in order to improve the results in the literature, it was desired to make the MnO₂ added carbon fabric more functional

with components such as two-dimensional MXene. For this purpose, MXene was added from a low amount (5 mg) to a high amount (15 mg) and the synthesis was carried out successfully. On the other hand, it was understood that the electrochemical performance was high in the highly doped sample, which would contribute to the literature. The possible reason for this increase is thought to be due to the synergistic effect of the two functional components together.

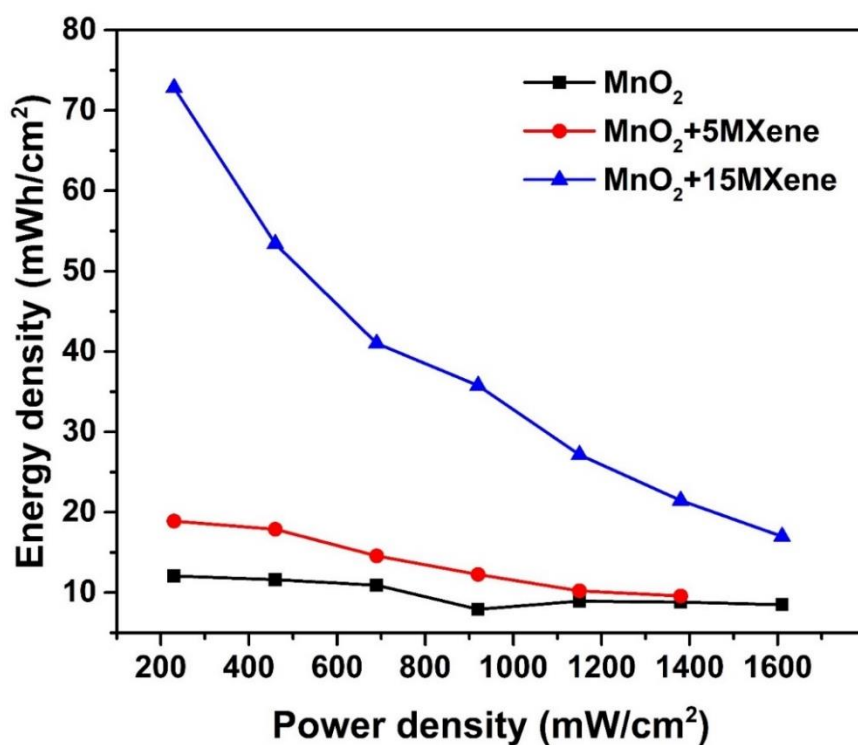


Figure 4.11. Energy and power density of electrodes

PART 5

SUMMARY

In this study, it is aimed to design an electrode for flexible energy storage devices. For this purpose, firstly, cotton fabric was carbonized and obtained both as conductive and flexible. Then, the surface of this fabric was functionalized by synthesizing MnO₂ by hydrothermal method. In addition, it is aimed to increase the performance of the electrode by adding two-dimensional MXene at different rates to this synthesis. All the above-mentioned sequences were carried out and the products were characterized by XRD, SEM and TEM. According to the results, MnO₂ crystals longer than 100 nm and smaller than 50 nm in diameter were successfully synthesized together with MXene in a layered structure on carbon fabric surfaces. The electrochemical performances of these prepared electrodes were investigated by cyclic voltammetry (CV) and galvanostatic charge-discharge (GCD) measurements. According to the results, the specific capacitance of the MnO₂ added fabric was 182 mF/cm', while the 5 mg and 15 mg MXene added fabrics were approximately 285 and 1100 mF/cm², respectively. According to these results, the MXene add-on increased the specific capacitance so much due to its large surface area and easy ion exchange. It has been concluded that the results will contribute to the literature but need to be examined in more detail.

REFERENCES

1. POLAT, S., "Dielectric Properties of BN-ZnO-GNP Doped PU-EG Composites", *International Journal Of Engineering Research And Development*, 13 (2): 635–644 (2021).
2. POLAT, S., "Dielectric Properties of GNPs@ MgO/CuO@ PVDF Composite Films", *Erciyes Üniversitesi Fen Bilimleri Enstitüsü Fen Bilimleri Dergisi*, 37 (3): 412–422 (2021).
3. Wang, H., Liang, Y., Mirfakhrai, T., Chen, Z., Casalongue, H. S., and Dai, H., "Advanced asymmetrical supercapacitors based on graphene hybrid materials", *Nano Research*, 4 (8): 729–736 (2011).
4. Wang, Q., Qin, B., Zhang, X., Wang, Y., Jin, L., and Cao, Q., "A green route to synthesize nitrogen-enriched graphene-like carbon nanosheets from bio-oil for supercapacitors", *Diamond And Related Materials*, 118: 108530 (2021).
5. Li, Y., Wang, L., Qu, Y., Wang, B., Yu, J., Song, D., Duan, C., and Yang, Y., "Unique 3D bilayer nanostructure basic cobalt carbonate@NiCo-layered double hydroxide nanosheets on carbon cloth for supercapacitor electrode material", *Ionics*, 26 (3): 1397–1406 (2020).
6. Ozen, A., Ozel, F., Kınas, Z., Karabiber, A., and Polat, S., "Spring assisted triboelectric nanogenerator based on sepiolite doped polyacrylonitrile nanofibers", *Sustainable Energy Technologies And Assessments*, 47: 101492 (2021).
7. Xue, Q., Sun, J., Huang, Y., Zhu, M., Pei, Z., Li, H., Wang, Y., Li, N., Zhang, H., and Zhi, C., "Recent progress on flexible and wearable supercapacitors", *Small*, 13 (45): 1701827 (2017).
8. Muzaffar, A., Ahamed, M. B., Deshmukh, K., and Thirumalai, J., "A review on recent advances in hybrid supercapacitors: Design, fabrication and applications", *Renewable And Sustainable Energy Reviews*, 101: 123–145 (2019).
9. Polat, S., "Production of ZnFe₂O₄ Doped Carbon Cloth-Based Flexible Composite Electrodes for Supercapacitors", *Türk Doğa Ve Fen Dergisi*, 10 (2): 199–205 (2021).
10. Niftaliyeva, A., Pehlivan, E., Polat, S., and Avci, A., "Chemical synthesis of single-layer graphene by using ball milling compared with NaBH₄ and hydroquinone reductants", *Micro & Nano Letters*, 13 (10): 1412–1416 (2018).
11. Gueon, D. and Moon, J. H., "MnO₂ nanoflake-shelled carbon nanotube particles for high-performance supercapacitors", *ACS Sustainable Chemistry & Engineering*, 5 (3): 2445–2453 (2017).
12. Shin, J., Seo, J. K., Yaylian, R., Huang, A., and Meng, Y. S., "A review on mechanistic understanding of MnO₂ in aqueous electrolyte for electrical energy storage systems", *International Materials Reviews*, 65 (6): 356–387 (2020).

13. Zhao, E., Qin, C., Jung, H.-R., Berdichevsky, G., Nese, A., Marder, S., and Yushin, G., "Lithium titanate confined in carbon nanopores for asymmetric supercapacitors", *ACS Nano*, 10 (4): 3977–3984 (2016).
14. Zou, K.-Y., Liu, Y.-C., Jiang, Y.-F., Yu, C.-Y., Yue, M.-L., and Li, Z.-X., "Benzoate acid-dependent lattice dimension of Co-MOFs and MOF-derived CoS₂@ CNTs with tunable pore diameters for supercapacitors", *Inorganic Chemistry*, 56 (11): 6184–6196 (2017).
15. Hu, C.-C., Chang, K.-H., Lin, M.-C., and Wu, Y.-T., "Design and Tailoring of the Nanotubular Arrayed Architecture of Hydrous RuO₂ for Next Generation Supercapacitors", *Nano Letters*, 6 (12): 2690–2695 (2006).
16. Cottineau, T., Toupin, M., Delahaye, T., Brousse, T., and Bélanger, D., "Nanostructured transition metal oxides for aqueous hybrid electrochemical supercapacitors", *Applied Physics A*, 82 (4): 599–606 (2006).
17. Polat, S. and Faris, D., "Fabrication of CuFe₂O₄@g-C₃N₄@GNPs nanocomposites as anode material for supercapacitor applications", *Ceramics International*, 48 (17): 24609–24618 (2022).
18. Toupin, M., Brousse, T., and Bélanger, D., "Charge Storage Mechanism of MnO₂ Electrode Used in Aqueous Electrochemical Capacitor", *Chemistry Of Materials*, 16 (16): 3184–3190 (2004).
19. Lu, X., Bai, Y., Wang, R., and Sun, J., "A high-performance flexible and weavable asymmetric fiber-shaped solid-state supercapacitor enhanced by surface modifications of carbon fibers with carbon nanotubes", *Journal Of Materials Chemistry A*, 4 (46): 18164–18173 (2016).
20. Xiong, S., Yuan, C., Zhang, X., Xi, B., and Qian, Y., "Controllable Synthesis of Mesoporous Co₃O₄ Nanostructures with Tunable Morphology for Application in Supercapacitors", *Chemistry – A European Journal*, 15 (21): 5320–5326 (2009).
21. Wei, W., Cui, X., Chen, W., and Ivey, D. G., "Manganese oxide-based materials as electrochemical supercapacitor electrodes", *Chemical Society Reviews*, 40 (3): 1697–1721 (2011).
22. Wang, J., Li, X., Zi, Y., Wang, S., Li, Z., Zheng, L., Yi, F., Li, S., and Wang, Z. L., "A flexible fiber-based supercapacitor–triboelectric-nanogenerator power system for wearable electronics", *Advanced Materials*, 27 (33): 4830–4836 (2015).
23. Zhang, Y., Cao, J., Yuan, Z., Zhao, L., Wang, L., and Han, W., "Assembling Co₃O₄ Nanoparticles into MXene with Enhanced electrochemical performance for advanced asymmetric supercapacitors", *Journal Of Colloid And Interface Science*, 599: 109–118 (2021).
24. Ali, G. A. M., Yusoff, M. M., Shaaban, E. R., and Chong, K. F., "High performance MnO₂ nanoflower supercapacitor electrode by electrochemical recycling of spent batteries", *Ceramics International*, 43 (11): 8440–8448 (2017).

25. Grote, F., Kühnel, R.-S., Balducci, A., and Lei, Y., "Template assisted fabrication of free-standing MnO₂ nanotube and nanowire arrays and their application in supercapacitors", *Applied Physics Letters*, 104 (5): 053904 (2014).
26. He, M., Cao, L., Li, W., Chang, X., and Ren, Z., " α -MnO₂ nanotube@ δ -MnO₂ nanoflake hierarchical structure on three-dimensional graphene foam as a lightweight and free-standing supercapacitor electrode", *Journal Of Alloys And Compounds*, 865: 158934 (2021).
27. Li, J., Yuan, X., Lin, C., Yang, Y., Xu, L., Du, X., Xie, J., Lin, J., and Sun, J., "Achieving High Pseudocapacitance of 2D Titanium Carbide (MXene) by Cation Intercalation and Surface Modification", *Advanced Energy Materials*, 7 (15): 1602725 (2017).
28. Xia, H., Feng, J., Wang, H., Lai, M. O., and Lu, L., "MnO₂ nanotube and nanowire arrays by electrochemical deposition for supercapacitors", *Journal Of Power Sources*, 195 (13): 4410–4413 (2010).
29. Mahmood, M., Rasheed, A., Ayman, I., Rasheed, T., Munir, S., Ajmal, S., Agboola, P. O., Warsi, M. F., and Shahid, M., "Synthesis of Ultrathin MnO₂ Nanowire-Intercalated 2D-MXenes for High-Performance Hybrid Supercapacitors", *Energy & Fuels*, 35 (4): 3469–3478 (2021).
30. Chu, J., Lu, D., Ma, J., Wang, M., Wang, X., and Xiong, S., "Controlled growth of MnO₂ via a facile one-step hydrothermal method and their application in supercapacitors", *Materials Letters*, 193: 263–265 (2017).
31. Garg, R., Agarwal, A., and Agarwal, M., "A review on MXene for energy storage application: effect of interlayer distance", *Materials Research Express*, 7 (2): 022001 (2020).
32. Hart, J. L., Hantanasirisakul, K., Lang, A. C., Anasori, B., Pinto, D., Pivak, Y., van Omme, J. T., May, S. J., Gogotsi, Y., and Taheri, M. L., "Control of MXenes' electronic properties through termination and intercalation", *Nature Communications*, 10 (1): 522 (2019).
33. Arun, T., Mohanty, A., Rosenkranz, A., Wang, B., Yu, J., Morel, M. J., Udayabhaskar, R., Hevia, S. A., Akbari-Fakhrabadi, A., Mangalaraja, R. V., and Ramadoss, A., "Role of electrolytes on the electrochemical characteristics of Fe₃O₄/MXene/RGO composites for supercapacitor applications", *Electrochimica Acta*, 367: 137473 (2021).
34. Naguib, M., Kurtoglu, M., Presser, V., Lu, J., Niu, J., Heon, M., Hultman, L., Gogotsi, Y., and Barsoum, M. W., "Two-Dimensional Nanocrystals Produced by Exfoliation of Ti₃AlC₂", *Advanced Materials*, 23 (37): 4248–4253 (2011).
35. Lukatskaya, M. R., Mashtalir, O., Ren, C. E., Dall'Agnese, Y., Rozier, P., Taberna, P. L., Naguib, M., Simon, P., Barsoum, M. W., and Gogotsi, Y., "Cation Intercalation and High Volumetric Capacitance of Two-Dimensional Titanium Carbide", *Science*, 341 (6153): 1502–1505 (2013).

36. Ghidui, M., Lukatskaya, M. R., Zhao, M.-Q., Gogotsi, Y., and Barsoum, M. W., "Conductive two-dimensional titanium carbide "clay" with high volumetric capacitance", *Nature*, 516 (7529): 78–81 (2014).
37. Li, K., Wang, X., Li, S., Urbankowski, P., Li, J., Xu, Y., and Gogotsi, Y., "An Ultrafast Conducting Polymer@MXene Positive Electrode with High Volumetric Capacitance for Advanced Asymmetric Supercapacitors", *Small*, 16 (4): 1906851 (2020).
38. Zhou, H., Lu, Y., Wu, F., Fang, L., Luo, H., Zhang, Y., and Zhou, M., "MnO₂ nanorods/MXene/CC composite electrode for flexible supercapacitors with enhanced electrochemical performance", *Journal Of Alloys And Compounds*, 802: 259–268 (2019).
39. Aïssa, B., Ali, A., Mahmoud, K. A., Haddad, T., and Nedil, M., "Transport properties of a highly conductive 2D Ti₃C₂T_x MXene/graphene composite", *Applied Physics Letters*, 109 (4): 043109 (2016).
40. Gangwar, D. and Rath, C., "Structural, optical and magnetic properties of α - and β -MnO₂ nanorods", *Applied Surface Science*, 557: 149693 (2021).
41. Xia, H., Wang, Y., Lin, J., and Lu, L., "Hydrothermal synthesis of MnO₂/CNT nanocomposite with a CNT core/porous MnO₂ sheath hierarchy architecture for supercapacitors", *Nanoscale Research Letters*, 7 (1): 33 (2012).
42. Hatakeyama, T., Okamoto, N. L., and Ichitsubo, T., "Thermal stability of MnO₂ polymorphs", *Journal Of Solid State Chemistry*, 305: 122683 (2022).
43. Chen, J., Wang, Y., He, X., Xu, S., Fang, M., Zhao, X., and Shang, Y., "Electrochemical properties of MnO₂ nanorods as anode materials for lithium ion batteries", *Electrochimica Acta*, 142: 152–156 (2014).
44. Shin, J., Seo, J. K., Yaylian, R., Huang, A., and Meng, Y. S., "A review on mechanistic understanding of MnO₂ in aqueous electrolyte for electrical energy storage systems", *International Materials Reviews*, 65 (6): 356–387 (2020).
45. Chemistry, L., .
46. Nawaz, F., Cao, H., Xie, Y., Xiao, J., Chen, Y., and Ghazi, Z. A., "Selection of active phase of MnO₂ for catalytic ozonation of 4-nitrophenol", *Chemosphere*, 168: 1457–1466 (2017).
47. Zhao, B., Ran, R., Wu, X., and Weng, D., "Phase structures, morphologies, and NO catalytic oxidation activities of single-phase MnO₂ catalysts", *Applied Catalysis A: General*, 514: 24–34 (2016).
48. Li, Y., Fan, Z., Shi, J., Liu, Z., and Shangguan, W., "Post plasma-catalysis for VOCs degradation over different phase structure MnO₂ catalysts", *Chemical Engineering Journal*, 241: 251–258 (2014).

49. Sunaina, Chand, P., Joshi, A., Lal, S., and Singh, V., "Effect of hydrothermal temperature on structural, optical and electrochemical properties of α -MnO₂ nanostructures for supercapacitor application", *Chemical Physics Letters*, 777: 138742 (2021).
50. Saputra, E., Muhammad, S., Sun, H., Ang, H. M., Tadé, M. O., and Wang, S., "Different Crystallographic One-dimensional MnO₂ Nanomaterials and Their Superior Performance in Catalytic Phenol Degradation", *Environmental Science & Technology*, 47 (11): 5882–5887 (2013).
51. Chen, J., Wang, Y., He, X., Xu, S., Fang, M., Zhao, X., and Shang, Y., "Electrochemical properties of MnO₂ nanorods as anode materials for lithium ion batteries", *Electrochimica Acta*, 142: 152–156 (2014).
52. Zhang, Y., Liu, H., Zhu, Z., Wong, K., Mi, R., Mei, J., and Lau, W., "A green hydrothermal approach for the preparation of graphene/ α -MnO₂ 3D network as anode for lithium ion battery", *Electrochimica Acta*, 108: 465–471 (2013).
53. Mathew, V., Lim, J., Kang, J., Gim, J., Rai, A. K., and Kim, J., "Self-assembled mesoporous manganese oxide with high surface area by ambient temperature synthesis and its enhanced electrochemical properties", *Electrochemistry Communications*, 13 (7): 730–733 (2011).
54. Teli, A. M., Bekanalkar, S. A., Patil, D. S., Pawar, S. A., Dongale, T. D., Shin, J. C., Kim, H. J., and Patil, P. S., "Effect of thermal annealing on physiochemical properties of spray-deposited β -MnO₂ thin films for electrochemical supercapacitor", *Journal Of Electroanalytical Chemistry*, 856: 113483 (2020).
55. Khazaei, M., Arai, M., Sasaki, T., Chung, C.-Y., Venkataramanan, N. S., Estili, M., Sakka, Y., and Kawazoe, Y., "Novel Electronic and Magnetic Properties of Two-Dimensional Transition Metal Carbides and Nitrides", *Advanced Functional Materials*, 23 (17): 2185–2192 (2013).
56. Zhang, X., Zhang, Z., and Zhou, Z., "MXene-based materials for electrochemical energy storage", *Journal Of Energy Chemistry*, 27 (1): 73–85 (2018).
57. Lei, J.-C., Zhang, X., and Zhou, Z., "Recent advances in MXene: Preparation, properties, and applications", *Frontiers Of Physics*, 10 (3): 276–286 (2015).
58. Naguib, M., Mochalin, V. N., Barsoum, M. W., and Gogotsi, Y., "25th Anniversary Article: MXenes: A New Family of Two-Dimensional Materials", *Advanced Materials*, 26 (7): 992–1005 (2014).
59. Eklund, P., Beckers, M., Jansson, U., Högberg, H., and Hultman, L., "The M+1AX phases: Materials science and thin-film processing", *Thin Solid Films*, 518 (8): 1851–1878 (2010).
60. Zhang, T., Zhang, L., and Hou, Y., "MXenes: Synthesis strategies and lithium-sulfur battery applications", *EScience*, 2 (2): 164–182 (2022).

61. Giménez, R., Serrano, B., San-Miguel, V., and Cabanelas, J. C., "Recent Advances in MXene/Epoxy Composites: Trends and Prospects", *Polymers*, 14 (6): 1170 (2022).
62. Barsoum, M. W., "MAX Phases: Properties of Machinable Ternary Carbides and Nitrides", *John Wiley & Sons*, 542 (2013).
63. Barsoum, M. W., El-Raghy, T., and Ali, M., "Processing and characterization of Ti₂AlC, Ti₂AlN, and Ti₂AlC_{0.5}N_{0.5}", *Metallurgical And Materials Transactions A*, 31 (7): 1857–1865 (2000).
64. Salim, O., Mahmoud, K. A., Pant, K. K., and Joshi, R. K., "Introduction to MXenes: synthesis and characteristics", *Materials Today Chemistry*, 14: 100191 (2019).
65. Naguib, M., Kurtoglu, M., Presser, V., Lu, J., Niu, J., Heon, M., Hultman, L., Gogotsi, Y., and Barsoum, M. W., "Two-Dimensional Nanocrystals Produced by Exfoliation of Ti₃AlC₂", *Advanced Materials*, 23 (37): 4248–4253 (2011).
- 66.
67. Naguib, M., Halim, J., Lu, J., Cook, K. M., Hultman, L., Gogotsi, Y., and Barsoum, M. W., "New Two-Dimensional Niobium and Vanadium Carbides as Promising Materials for Li-Ion Batteries", *Journal Of The American Chemical Society*, 135 (43): 15966–15969 (2013).
68. Halim, J., Lukatskaya, M. R., Cook, K. M., Lu, J., Smith, C. R., Näslund, L.-Å., May, S. J., Hultman, L., Gogotsi, Y., Eklund, P., and Barsoum, M. W., "Transparent Conductive Two-Dimensional Titanium Carbide Epitaxial Thin Films", *Chemistry Of Materials*, 26 (7): 2374–2381 (2014).
69. Ghidui, M., Lukatskaya, M. R., Zhao, M.-Q., Gogotsi, Y., and Barsoum, M. W., "Conductive two-dimensional titanium carbide "clay" with high volumetric capacitance", *Nature*, 516 (7529): 78–81 (2014).
70. Naguib, M., Mashtalir, O., Lukatskaya, M. R., Dyatkin, B., Zhang, C., Presser, V., Gogotsi, Y., and Barsoum, M. W., "One-step synthesis of nanocrystalline transition metal oxides on thin sheets of disordered graphitic carbon by oxidation of MXenes", *Chem. Commun.*, 50 (56): 7420–7423 (2014).
71. Li, Z., Wang, L., Sun, D., Zhang, Y., Liu, B., Hu, Q., and Zhou, A., "Synthesis and thermal stability of two-dimensional carbide MXene Ti₃C₂", *Materials Science And Engineering: B*, 191: 33–40 (2015).
72. Li, J., Du, Y., Huo, C., Wang, S., and Cui, C., "Thermal stability of two-dimensional Ti₂C nanosheets", *Ceramics International*, 41 (2, Part A): 2631–2635 (2015).
73. Liu, K., Xia, Q., Si, L., Kong, Y., Shinde, N., Wang, L., Wang, J., Hu, Q., and Zhou, A., "Defect engineered Ti₃C₂T_x MXene electrodes by phosphorus doping

- with enhanced kinetics for supercapacitors", *Electrochimica Acta*, 435: 141372 (2022).
74. Yang, W., Han, Q., Li, W., Wu, M., Yao, J., Zhao, M., and Lu, X., "Ti₃C₂T_x MXene as Janus separators for redox-enhanced electrochemical capacitors with reduced self-discharge", *Energy Storage Materials*, 52: 29–39 (2022).
 75. Zhang, X., Zhang, W., and Zhao, H., "Electrochemical performance of Ti₃C₂T_x MXenes obtained via ultrasound assisted LiF-HCl method", *Materials Today Communications*, 33: 104384 (2022).
 76. Jino, L., Dev Prasad, V., Ajay Eswar, M., Manoj, E., Jacob, A., Arockia Suthan, S., Jayaganthan, A., and Anderson, A., "Review on natural fibre composites reinforced with nanoparticles", *Materials Today: Proceedings*, (2023).
 77. Khan, I., Saeed, K., and Khan, I., "Nanoparticles: Properties, applications and toxicities", *Arabian Journal Of Chemistry*, 12 (7): 908–931 (2019).
 78. Khitab, A., Ahmad, S., Munir, M. J., Kazmi, S. M. S., Arshad, T., and Khushnood, R. A., "Synthesis and Applications of Nano Titania Particles: A Review", *REVIEWS ON ADVANCED MATERIALS SCIENCE*, 53 (1): 90–105 (2018).
 79. Swihart, M. T., "Vapor-phase synthesis of nanoparticles", *Current Opinion In Colloid & Interface Science*, 8 (1): 127–133 (2003).
 80. Flagan, R. C. and Lunden, M. M., "Particle structure control in nanoparticle synthesis from the vapor phase", *Materials Science And Engineering A*, 204 (1–2): 113–124 (1995).
 81. Flagan, R. C. and Lunden, M. M., "Particle structure control in nanoparticle synthesis from the vapor phase", *Materials Science And Engineering A*, 204 (1–2): 113–124 (1995).
 82. Mattox, D. M., "Physical vapor deposition (PVD) processes", *Metal Finishing*, 100: 394–408 (2002).
 83. Helmersson, U., Lattemann, M., Bohlmark, J., Ehiasarian, A. P., and Gudmundsson, J. T., "Ionized physical vapor deposition (IPVD): A review of technology and applications", *Thin Solid Films*, 513 (1–2): 1–24 (2006).
 84. Donadt, T. B. and Yang, R., "Vapor-Deposited Biointerfaces and Bacteria: An Evolving Conversation", *ACS Biomaterials Science & Engineering*, 6 (1): 182–197 (2020).
 - 85.
 86. Schwander, M. and Partes, K., "A review of diamond synthesis by CVD processes", *Diamond And Related Materials - DIAM RELAT MATER*, 20: 1287–1301 (2011).

87. Bayer, E. and Mutter, M., "Liquid Phase Synthesis of Peptides", *Nature*, 237 (5357): 512–513 (1972).
88. Miao, W. and Chan, T. H., "Ionic-Liquid-Supported Synthesis: A Novel Liquid-Phase Strategy for Organic Synthesis", *Accounts Of Chemical Research*, 39 (12): 897–908 (2006).
89. Semagina, N. and Kiwi-Minsker, L., "Recent Advances in the Liquid-Phase Synthesis of Metal Nanostructures with Controlled Shape and Size for Catalysis", *Catalysis Reviews*, 51 (2): 147–217 (2009).
90. Mantzaris, N. V., "Liquid-phase synthesis of nanoparticles: Particle size distribution dynamics and control", *Chemical Engineering Science*, 60 (17): 4749–4770 (2005).
91. Chen, C. and Chen, Y.-J., "Liquid-phase synthesis of 2-substituted benzimidazoles, benzoxazoles and benzothiazoles", *Tetrahedron Letters*, 45 (1): 113–115 (2004).
92. Yang, G. and Park, S.-J., "Conventional and Microwave Hydrothermal Synthesis and Application of Functional Materials: A Review", *Materials*, 12 (7): 1177 (2019).
93. Hayashi, H. and Hakuta, Y., "Hydrothermal Synthesis of Metal Oxide Nanoparticles in Supercritical Water", *Materials*, 3 (7): 3794–3817 (2010).
94. Morey, G. W., "Hydrothermal Synthesis", *Journal Of The American Ceramic Society*, 36 (9): 279–285 (1953).
95. Zhou, Q., Du, D., Lu, C., He, Q., and Liu, W., "A review of thermal energy storage in compressed air energy storage system", *Energy*, 188: 115993 (2019).
96. Yang, Y., Bremner, S., Menictas, C., and Kay, M., "Battery energy storage system size determination in renewable energy systems: A review", *Renewable And Sustainable Energy Reviews*, 91: 109–125 (2018).
97. Chen, H., Cong, T. N., Yang, W., Tan, C., Li, Y., and Ding, Y., "Progress in electrical energy storage system: A critical review", *Progress In Natural Science*, 19 (3): 291–312 (2009).
98. Chiang, S. J., Chang, K. T., and Yen, C. Y., "Residential photovoltaic energy storage system", *IEEE Transactions On Industrial Electronics*, 45 (3): 385–394 (1998).
99. Vieira, F. M., Moura, P. S., and de Almeida, A. T., "Energy storage system for self-consumption of photovoltaic energy in residential zero energy buildings", *Renewable Energy*, 103: 308–320 (2017).
100. Wang, S., Zhang, X., Yang, L., Zhou, Y., and Wang, J., "Experimental study of compressed air energy storage system with thermal energy storage", *Energy*, 103: 182–191 (2016).

101. Qu, D. and Shi, H., "Studies of activated carbons used in double-layer capacitors", *Journal Of Power Sources*, 74 (1): 99–107 (1998).
102. Şahin, M. E., Blaabjerg, F., and Sangwongwanich, A., "A Comprehensive Review on Supercapacitor Applications and Developments", *Energies*, 15 (3): 674 (2022).
103. Zhang, L. L. and Zhao, X. S., "Carbon-based materials as supercapacitor electrodes", *Chemical Society Reviews*, 38 (9): 2520 (2009).
104. Gao, D., "Improvement of Chen-Zhang-Liu's IRPB Signature Scheme", *Intelligent Information Management*, 02 (09): 559–562 (2010).
105. Sarangapani, S., "Materials for Electrochemical Capacitors", *J. Electrochem. Soc.*, 143 (11): (1996).
106. Ding, J., Hu, W., Paek, E., and Mitlin, D., "Review of Hybrid Ion Capacitors: From Aqueous to Lithium to Sodium", *Chemical Reviews*, (2018).
107. Arvas, M. B., Yazar, S., and Sahin, Y., "Electrochemical synthesis and characterization of self-doped aniline 2-sulfonic acid-modified flexible electrode with high areal capacitance and rate capability for supercapacitors", *Synthetic Metals*, 285: 117017 (2022).
108. Beidaghi, M. and Gogotsi, Y., "Capacitive energy storage in micro-scale devices: recent advances in design and fabrication of micro-supercapacitors", *Energy & Environmental Science*, 7 (3): 867–884 (2014).
109. Decker, A., "Solar energy harvesting for autonomous field devices", *IET Wireless Sensor Systems*, 4 (1): 1–8 (2014).
110. Jayasinghe, S. D. G. and Vilathgamuwa, D. M., "Flying supercapacitors as power smoothing elements in wind generation", *IEEE Transactions On Industrial Electronics*, 60 (7): 2909–2918 (2013).
111. Zhang, L., Hu, X., Wang, Z., Sun, F., Deng, J., and Dorrell, David. G., "Multiobjective Optimal Sizing of Hybrid Energy Storage System for Electric Vehicles", *IEEE Transactions On Vehicular Technology*, 67 (2): 1027–1035 (2018).
112. Lahyani, A., Venet, P., Guermazi, A., and Troudi, A., "Battery/Supercapacitors Combination in Uninterruptible Power Supply (UPS)", *IEEE Transactions On Power Electronics*, 28 (4): 1509–1522 (2013).
113. Pandey, A., Allos, F., Hu, A. P., and Budgett, D., "Integration of supercapacitors into wirelessly charged biomedical sensors", *2011 6th IEEE Conference on Industrial Electronics and Applications*, (2011).
114. Stoller, M. D. and Ruoff, R. S., "Best practice methods for determining an electrode material's performance for ultracapacitors", *Energy & Environmental Science*, 3 (9): 1294–1301 (2010).

115. Zhang, S. and Pan, N., "Supercapacitors Performance Evaluation", *Advanced Energy Materials*, 5 (6): 1401401 (2015).
116. Taberna, P. L., Simon, P., and Fauvarque, J. F., "Electrochemical characteristics and impedance spectroscopy studies of carbon-carbon supercapacitors", *Journal Of The Electrochemical Society*, 150 (3): A292–A300 (2003).
117. González, A., Goikolea, E., Barrena, J. A., and Mysyk, R., "Review on supercapacitors: Technologies and materials", *Renewable And Sustainable Energy Reviews*, 58: 1189–1206 (2016).
118. Li, X., Lin, Z., Wei, Y., Luo, W., Ding, J., Li, T., and Ma, Y., "MXene-MnO₂-CoNi layered double hydroxides//activated carbon flexible asymmetric supercapacitor", *Journal Of Energy Storage*, 55: 105668 (2022).
119. Dong, X., Wang, X., Wang, J., Song, H., Li, X., Wang, L., Chan-Park, M. B., Li, C. M., and Chen, P., "Synthesis of a MnO₂-graphene foam hybrid with controlled MnO₂ particle shape and its use as a supercapacitor electrode", *Carbon*, 50 (13): 4865–4870 (2012).
120. Shaikh, Z. A., Shinde, P. V., Shaikh, S. F., Al-Enizi, A. M., and Mane, R. S., "Facile synthesis of Bi₂O₃@MnO₂ nanocomposite material: A promising electrode for high performance supercapacitors", *Solid State Sciences*, 102: 106158 (2020).
121. Kumari, S. and Bhatia, D., "Design of hydroxylated MnO₂ nano-bricks for high-performance supercapacitors", *Materials Today: Proceedings*, 58: 523–528 (2022).
122. Jiao, K., Suo, J., Pan, C., Khamidov, A., Ruzimuradov, O., Wang, M., Fang, D., and Li, C., "Facile in-situ synthesis of MnO₂-ITO NWs composite for electrochemical supercapacitors", *Solid State Ionics*, 388: 116080 (2022).
123. Zhao, Y., Zhu, Z., Wang, A., Xiao, L., and Hou, L., "Facile synthesis of N, S co-doped hierarchical porous carbon/MnO₂ composites for supercapacitor electrodes via sodium alginate crosslinking", *Journal Of Alloys And Compounds*, 923: 166333 (2022).
124. Kiymaz, D., Kiymaz, A., Tekoglu, S., Mayr, F., Dincalp, H., and Zafer, C., "Charge transport kinetics in flower like α -MnO₂ nano-sheet and α -MnO₂ nanowire based supercapacitors", *Thin Solid Films*, 762: 139535 (2022).
125. Jiang, J. and Kucernak, A., "Electrochemical supercapacitor material based on manganese oxide: preparation and characterization", *Electrochimica Acta*, 47 (15): 2381–2386 (2002).
126. Chen, B., Song, Q., Zhou, Z., and Lu, C., "A Novel Sandwiched Porous MXene/Polyaniline Nanofibers Composite Film for High Capacitance Supercapacitor Electrode", *Advanced Materials Interfaces*, 8 (12): 2002168 (2021).

127. Wu, W., Lin, S., Chen, T., Li, L., Pan, Y., Zhang, M., Wu, L., Gao, H., and Zhang, X., "Performance evaluation of asymmetric supercapacitor based on Ti₃C₂T_x-paper", *Journal Of Alloys And Compounds*, 729: 1165–1171 (2017).
128. Ma, R., Zhang, X., Zhuo, J., Cao, L., Song, Y., Yin, Y., Wang, X., Yang, G., and Yi, F., "Self-Supporting, Binder-Free, and Flexible Ti₃C₂T_x MXene-Based Supercapacitor Electrode with Improved Electrochemical Performance", *ACS Nano*, (2022).
129. Wang, R., Zhang, T., Cheng, X., Xiao, J., and Gao, H., "Ti₃C₂T_x aerogel with 1D unidirectional channels for high mass loading supercapacitor electrodes", *Ceramics International*, 48 (14): 20324–20331 (2022).
130. Javed, M. S., Zhang, X., Ali, S., Mateen, A., Idrees, M., Sajjad, M., Batool, S., Ahmad, A., Imran, M., Najam, T., and Han, W., "Heterostructured bimetallic–sulfide@layered Ti₃C₂T_x–MXene as a synergistic electrode to realize high-energy-density aqueous hybrid-supercapacitor", *Nano Energy*, 101: 107624 (2022).
131. Khitab, A., Ahmad, S., Munir, M. J., Kazmi, S. M. S., Arshad, T., and Khushnood, R. A., "Synthesis and Applications of Nano Titania Particles: A Review", *REVIEWS ON ADVANCED MATERIALS SCIENCE*, 53 (1): 90–105 (2018).
132. Xiao, W., Xia, H., Fuh, J. Y. H., and Lu, L., "Growth of single-crystal α -MnO₂ nanotubes prepared by a hydrothermal route and their electrochemical properties", *Journal Of Power Sources*, 193 (2): 935–938 (2009).
133. Zhou, H., Lu, Y., Wu, F., Fang, L., Luo, H., Zhang, Y., and Zhou, M., "MnO₂ nanorods/MXene/CC composite electrode for flexible supercapacitors with enhanced electrochemical performance", *Journal Of Alloys And Compounds*, 802: 259–268 (2019).
134. Nagarajan, N., Humadi, H., and Zhitomirsky, I., "Cathodic electrodeposition of MnO_x films for electrochemical supercapacitors", *Electrochimica Acta*, 51 (15): 3039–3045 (2006).
135. Ranjithkumar, R., Arasi, S. E., Sudhakar, S., Nallamuthu, N., Devendran, P., Lakshmanan, P., and Kumar, M. K., "Enhanced electrochemical studies of ZnO/CNT nanocomposite for supercapacitor devices", *Physica B: Condensed Matter*, 568: 51–59 (2019).
136. Zhang, S., Gao, H., Zhou, J., Jiang, F., and Zhang, Z., "Hydrothermal synthesis of reduced graphene oxide-modified NiCo₂O₄ nanowire arrays with enhanced reactivity for supercapacitors", *Journal Of Alloys And Compounds*, 792: 474–480 (2019).
137. Polat, S. and Faris, D., "Fabrication of CuFe₂O₄@g-C₃N₄@GNPs nanocomposites as anode material for supercapacitor applications", *Ceramics International*, 48 (17): 24609–24618 (2022).

138. He, Y., Zhang, Y., Li, X., Lv, Z., Wang, X., Liu, Z., and Huang, X., "Capacitive mechanism of oxygen functional groups on carbon surface in supercapacitors", *Electrochimica Acta*, 282: 618–625 (2018).
139. Mashrah, M. and Polat, S., "Hydrothermal synthesis and electrochemical performance of GNPs-doped MgFe₂O₄ electrodes for supercapacitors", *Solid State Ionics*, 391: 116107 (2023).
140. Polat, S. and Mashrah, M., "Synthesis and electrochemical performance of MgFe₂O₄ with g-C₃N₄ on Ni-foam as composite anode material in supercapacitors", *Journal Of Materials Science: Materials In Electronics*, 33 (30): 23427–23436 (2022).

RESUME

Mariem ABDI completed her primary, secondary and undergraduate education in Mauritania. She graduated from EL MAARIF School in Nouakchott in 2016 and started her education at UNIVERSITY OF NOUAKCHOTT ALASRIYA in the department of geology and graduated in 2019. In 2020 she started her education as a graduate student at Karabuk University (INSTITU OF APPLIED SCIENCE) Department of Metallurgy and material engineering.